Barrier islands face a gradual path toward drowning under most sea level rise scenarios

Laura Portos-Amill[1]*, Jaap H. Nienhuis[2], Huib E. de Swart[1]

[1]Institute for Marine and Atmospheric Research, Department of Physics, Utrecht University, NL
[2]Department of Physical Geography, Utrecht University, NL

Key Points:

- Rapid sea level rise makes inlets expand until barrier islands disappear
- Barrier drowning lags increases in rates of sea level rise by hundreds of years
- Higher rates of sea level rise cause earlier, intensified drowning while higher waves cause more drowning or more frequent inlet closure

*Now at Water and Engineering Management, University of Twente, Enschede, NL

Corresponding author: Laura Portos-Amill, `l.portosamill@utwente.nl`

Abstract

The expected increase in rates of sea level rise during the 21st century and beyond may cause tidal inlets to expand and barrier islands to drown. However, many aspects remain unclear, e.g., the timescales involved in the drowning process have received little attention. To gain insight into the morphodynamics of barrier systems subject to sea level rise, we here present results obtained with a novel barrier island model, BRIE-D. This new model allows for changes in the alongshore extent of the barrier lying below sea level. These concern reductions in barrier width, barrier height, as well as lateral expansion of tidal inlets. Model results show that the evolution of barrier islands is susceptible to the wave height and the rate of sea level rise that they experience. It takes hundreds of years for barrier islands to drown in response to high rates of sea level rise (more than 15 mm/yr). Furthermore, increasing rates of sea level rise cause an earlier and more severe barrier drowning in environments with low waves. Barrier systems that face higher waves can undergo more frequent inlet closures (due to a larger amount of sediment imported into the inlets), but also the degree of barrier drowning might increase (due to a deepening of the toe of the shoreface). The latter process dominates over the former when rates of sea level rise are higher than 5 mm/yr.

Plain Language Summary

Barrier islands respond to an increase in sea level by migrating landward. Furthermore, inlet width and/or number may increase as portions of the barrier drown. In extreme sea level rise scenarios (like those predicted during the 21st century and beyond) barrier islands may not be able to migrate landward fast enough to keep up with sea level rise. In these situations, barrier islands will (partially) drown. Nowadays, it is difficult to predict when and under which conditions this drowning may occur. To better understand the dynamics of a drowning barrier island, we adapted a pre-existing numerical model. The new aspects of the model are that inlet widths may change gradually, depending on the barrier response to sea level rise and sediment availability. It was found that rates of sea level rise and the height of incoming waves are the key drivers that determine the long-term fate of barrier systems. Higher rates of sea level rise result in a larger portion of the barrier that is drowned. When wave heights are increased, the inlets tend to close more easily (when rates of sea level rise are small to moderate, i.e., less than 5 mm/yr), or there is more drowning (for higher rates of sea level rise).

1 Introduction

Barrier islands are low-lying coastal land forms that constitute $10-15\%$ of the world's coasts. They lie parallel to the mainland coast, thereby they protect it from coastal hazards such as storm surges (FitzGerald et al., 2006). As most coastal lowlands are densely populated, they are thus of great socio-economic importance.

Most barrier islands were created during the Holocene, when rates of sea level rise (SLR) decreased from $7-15$ mm/yr to ~ 2 mm/yr (Leatherman, 1983; Beets & van der Spek, 2000; Mariotti, 2021). With this change, sediment deposition could gradually catch up with SLR and compensate for its creation of accommodation. If all inlets filled up, then uninterrupted barrier coasts were formed. However, in some areas sediment supply was insufficient to fill up the inlets completely, then barrier islands were formed. The latter was the case of the Wadden Islands along the Dutch, German and Danish coast, which formed around 7000 yrs BP (Beets & van der Spek, 2000), as well as that of the barrier islands along the US east coast (Figure 1).

Future projected SLR is an important threat to most coastal systems in the world. Worst case scenarios predict a global mean sea level (MSL) increase of roughly 2.7 m by the year 2300 with respect to that of the year 2000 (Palmer et al., 2020). Furthermore,

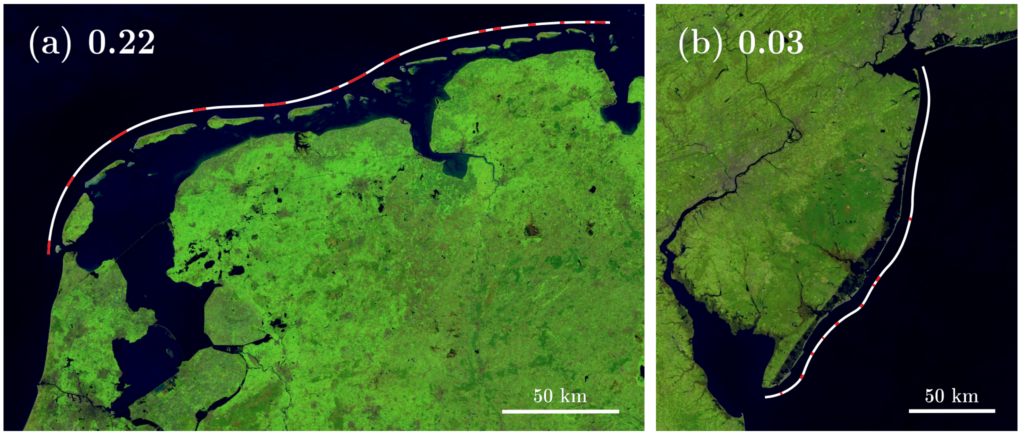

Figure 1. Examples of barrier islands and their respective fraction below mean sea level: **(a)** 0.22 for the Wadden Islands along the coasts of the Netherlands and Germany, and **(b)** 0.03 for the barrier islands along the US east coast of New Jersey. White curves represent the islands extent, while red curves represent that of inlets. The given fraction below MSL is computed as the ratio between inlet extent and the total barrier chain extent (inlets and islands). Extracted from Google Earth (images provided by TerraMetrics).

the effects of e.g., vertical land motion should also be considered when studying the response of coastal systems to changes in sea level. Given that many barrier islands are located near deltas, where land is sinking, they may experience high relative rates of SLR. Another possible consequence of climate change are variations in storm return periods, which can also affect barrier coasts through changes in barrier breaching and sediment transport during overwash events (Reef et al., 2020).

One of the possible consequences of this increase in sea level, is that barrier islands will not be able to migrate landward fast enough, thus resulting in “whole scale” barrier island drowning (Gilbert, 1885; Storms et al., 2002; Lorenzo-Trueba & Ashton, 2014; Mellett & Plater, 2018; Nienhuis & Lorenzo-Trueba, 2019a). Observations of drowning of barrier systems as a whole are scarce. There is an example in the English Channel, where a barrier was formed around 9500−8800 yrs BP, when MSL was at −22 m relative to that of present day, and it drowned around 8300 yrs BP when MSL reached −17 m (Sanders & Kumar, 1975).

Partial barrier drowning is more common. With high rates of SLR, the fraction of a barrier island chain lying below MSL (inlets, see Figure 1) is expected to increase. More inlets are formed or existing inlets become wider (FitzGerald et al., 2018). Inlets that might have been in equilibrium, due to a balance between sediment export by tidal currents and sediment import by littoral drift (Escoffier, 1940), will deviate from that equilibrium when the MSL changes. An example of such a situation is the evolution of the Isles Dernières, Louisiana since the mid-1800s. At that time, a drowning process started to take place, resulting in narrowing of the barrier and creation of new inlets, as well as widening of existing inlets (FitzGerald et al., 2008).

In part because of the scarcity of observations, we remain unable to predict when and where barriers will drown. Modern barrier islands might be at equilibrium with the tides and waves, but they might also already show signs of drowning. The timescales involved in barrier island drowning from present-day SLR are mostly unknown, and could be long (Mariotti & Hein, 2022).

Models have been developed to better understand barrier dynamics, and barrier drowning. Cowell et al. (1992) developed a cross-shore model that describes the evolution of the active shoreface profile subject to SLR and to losses and gains of sediment beyond the active profile. Masetti et al. (2008) developed a more detailed cross-shore model, where additional sediment dynamics are included. Their model is able to represent overwash, eolian processes, and sediment input from rivers in the back-barrier lagoon. This model was used to study the dependency of barrier island drowning on overwash fluxes. Lorenzo-Trueba and Ashton (2014) also designed a cross-shore model to study barrier island drowning and retreat due to SLR. Their model uses a more idealized domain than that of Masetti et al. (2008), but is able to represent different dynamic equilibrium configurations of the barrier.

These cross-sectional models can represent the process of barrier drowning, but to study chains of barrier islands, two horizontal dimensions are required. Such models have been recently developed (Ashton & Lorenzo-Trueba, 2018; Nienhuis & Lorenzo-Trueba, 2019b; Mariotti, 2021). The model by Ashton and Lorenzo-Trueba (2018) follows the same parameterized cross-shore dynamics as that of Lorenzo-Trueba and Ashton (2014), and couples them in the alongshore direction with a shoreline diffusivity. The BRIE model of Nienhuis and Lorenzo-Trueba (2019b) presents a more realistic picture by also accounting for inlet dynamics. Similarly, the model of Mariotti (2021) also accounts for inlet dynamics, but uses a more process-based approach. The advantage of the parameterized BRIE model is that it is fast, so it is a suitable tool for performing extensive sensitivity studies. Furthermore, since it explicitly accounts for inlet dynamics, such as opening, closing, or migration, it can offer insights into partial drowning, where only a fraction of the chain is below sea level. Tidal inlets in BRIE, however, cannot expand beyond their equilibrium state, and therefore the model struggles to appropriately quantify the effect of SLR on the size and/or number of inlets.

Motivated by these knowledge gaps, we modify and expand the BRIE model into the BRIE-D model to allow for SLR-driven transformations of tidal inlets on barrier island chains. The new aspects implemented in the BRIE-D model concern a better representation of the process of inlet expansion, therefore allowing a gradual increase in the alongshore extent of the barrier lying below MSL. The evolution of the inlet width depends on the distribution of alongshore sediment transport within the inlet, the exchange of sediment with the flood-tidal delta, merging with other inlets, and drowning of portions of the barrier.

Our study objectives are to (1) understand how the fraction of the barrier lying below MSL is affected by SLR-driven inlet widening by comparing the outcomes of the BRIE model with those of the BRIE-D model, (2) examine the temporal evolution of the fraction of the barrier that is drowned, as well as to quantify drowning timescales, and (3) explore the dependence of barrier island drowning on model parameters.

The next section includes the model description, design of simulations and analysis of model output. Section 3 contains the results, followed by a discussion in Section 4. The final section contains the conclusions.

2 Methods

2.1 Model Description

Here we give an overview of the physics represented in the BRIE-D model, with a detailed model description and relevant equations given in the Supplementary Infor-

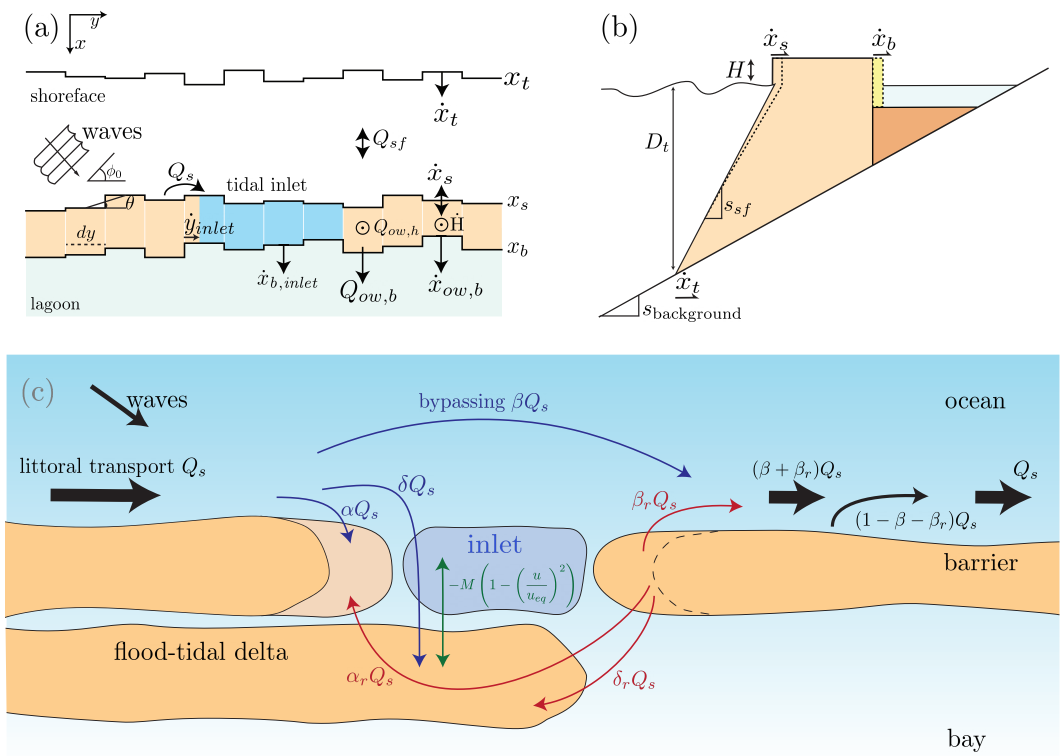

Figure 2. Schematized model domain: **(a)** plan view highlighting the three moving boundaries (toe of the shoreface x_t, shoreline x_s and back-barrier shoreline x_b) and barrier height H, as well as the sediment transports determining their evolution. Vectors indicate the direction of potential changes, with the dot symbolizing barrier heightening. We use $\dot{x}$ to represent the local time derivative. **(b)** Cross-shore view of the barrier showing landward migration in terms of $\dot{x}_s$ and $\dot{x}_b$. **(c)** Mass balance of the boxes used in modeling inlet dynamics, including sediment exchange with updrift and downdrift tips of the barrier, as well as with the flood-tidal delta. The parameters α, β, δ, α_r, β_r and δ_r denote fractions of the littoral transport Q_s. Note that the flood-tidal delta extends through the updrift barrier because it has been building up as the inlet was migrating. Modified from Nienhuis and Lorenzo-Trueba (2019b) and Nienhuis and Ashton (2016). A detailed description on the moving boundaries and the sediment exchange within the inlet is given in SI1.

mation (SI1). Differences between the BRIE-D and the BRIE model involve the inlet evolution (Section 2.1.4), all other routines are equivalent in both models.

2.1.1 Domain

The BRIE-D model uses an idealized model domain with the $x-$ and $y-$ axis pointing perpendicular and parallel to the barrier, respectively. The $z-$ axis points upward, with $z = 0$ representing MSL at $t = 0$. The domain comprises the shoreface, the subaerial part of the barrier, as well as the back-barrier lagoon (see Figure 2).

The model is driven by tides (with a prescribed range), rate of SLR and waves that propagate from deep water toward the barrier, among other boundary conditions. The waves are characterized by a significant wave height (assumed to be constant) and by an angle of incidence with respect to the $y-$axis. This angle is a stochastic variable that is determined by a probability density distribution that depends on wave asymmetry (fraction of waves approaching from the left, looking offshore) and wave highness (fraction of waves approaching at a high angle, i.e., $|\phi_0| > 45°$, see Figure 2a).

2.1.2 Cross-shore Dynamics

The BRIE-D model describes the barrier system in the cross-shore direction as the time evolution of barrier height and the location of three boundaries: the toe of the shoreface, and the shorelines of the barrier on the sea side, x_s, and back-barrier side, x_b. We define the toe of the shoreface as the location $x = x_t$ where there is negligible cross-shore sediment exchange between the shoreface and the shelf (Ortiz & Ashton, 2016). This corresponds to a depth $z = -D_t$ at $t = 0$. The depth of closure is set to $D_t = 8.9H_s$, so it depends on the significant wave height H_s at deep water (Houston, 1995), which is held constant in time in our simulations.

The cross-shore depth profile of the shoreface tends toward a prescribed equilibrium defined by the balance between onshore sediment transport by waves and offshore directed transport due to gravity. The shoreface sediment transport Q_{sf} is directed offshore when the bottom slope of the shoreface s_{sf} is larger than the equilibrium slope $s_{sf,eq}$, otherwise it is directed onshore. As revealed by Figure 2, $s_{sf} = D_t/(x_s - x_t)$, where $x = x_t$ and $x = x_s$ are the cross-shore positions of the toe of the shoreface and of the seaward shoreline of the barrier, respectively. Furthermore, $s_{sf,eq}$ is determined by the long-term wave conditions. The transport Q_{sf} is one of the drivers that determine time changes in both x_t and x_s (see SI1 for details). SLR is a second driver of changes in x_t, and it causes a decrease in barrier height H.

Sediment transport during overwash connects the shoreface with the back-barrier lagoon. Part of the sediment overwash accumulates on top of the barrier ($Q_{ow,h}$) and part of it is deposited in the back-barrier lagoon ($Q_{ow,b}$). The first contribution results in an increase in the height H of the barrier, while the latter results in an landward migration of the back-barrier shoreline, denoted by $x = x_b$. Both sediment overwash transport fluxes scale with their associated deficit volumes, which represent the difference between a current barrier configuration and one that is both high and wide enough such that overwash is presumed not to occur. The latter situation is characterized by the critical barrier width and critical barrier height (Jiménez & Sánchez-Arcilla, 2004; Lorenzo-Trueba & Ashton, 2014).

2.1.3 Inlet Opening

Inlets may open due to barrier breaching caused by a storm or due to barrier drowning. Breaching is imposed every 10 yrs where the barrier volume is at a minimum, and at a location at least 5 km from existing inlets. Alternatively, inlets appear when a portion of the barrier drowns (either because the width or the height of the barrier becomes negative), which is not restricted to its proximity to other inlets. We set the initial width of a breached inlet to 1 km, while for a drowned inlet we set it to the width of the portion of the barrier that drowned.

2.1.4 Inlet Evolution

We depart from the formulation used in the BRIE model by allowing for variations in the cross-sectional area of the inlet. In the BRIE model, the inlets were assumed to instantly attain their equilibrium cross-sectional area (following Escoffier, 1940). In the BRIE-D model, we impose a gradual temporal evolution of the inlet size. We distinguish between four different sources of variations in the cross-sectional area of the inlet A_{inlet},

$$\frac{dA_{inlet}}{dt} = G_{sd} + G_{Esc} + G_m + G_d \ , \tag{1}$$

where G_{sd} represents the variations due to the distribution of the alongshore transport within the inlet, G_{Esc} represents the changes in cross-sectional area due to sediment exchange between the inlet and the flood-tidal delta (which is partly parameterized following the theory by Escoffier, 1940), and G_m and G_d account for the increase in the cross-sectional area of the inlet due to merging with another inlet and due to drowning of the barrier, respectively.

Each inlet receives an amount of sediment per time unit that is a fraction of the alongshore sediment transport Q_s, where the latter depends on wave climate and shoreline angle. A fraction β of Q_s bypasses sediment to the coast of the downdrift island, another fraction δ toward the flood tidal delta, where the sediment gets deposited. The remaining fraction α transports sediment to the tip of the updrift island, where sediment gets deposited (see Figure 2c). Sediment eroded from the tip of the downdrift island is distributed similarly. This sediment distribution, which depends on tidal prism and wave characteristics, causes inlet migration and variations in the volume of the downdrift and updrift tips of the barrier, V_{down} and V_{up}, respectively. These variations in volume of the barrier cause changes in the cross-sectional area of the inlet,

$$G_{sd} = D_{inlet}\left(\frac{1}{A_{b,down}}\frac{dV_{down}}{dt} - \frac{1}{A_{b,up}}\frac{dV_{up}}{dt}\right) \ . \tag{2}$$

Here, $A_{b,down}$ and $A_{b,up}$ correspond to the cross-sectional area of the barrier downdrift and updrift of the inlet, and D_{inlet} represents the inlet depth. In the BRIE model this sediment distribution was such that the cross-sectional area of the inlet was maintained constant. Differently, in the BRIE-D model we allow for both tips of the barrier to be disconnected, and grow or shrink the inlet. A detailed description of the variations in updrift and downdrift volumes is given in SI1.

We also allow for variations in the cross-sectional area of the inlet depending on the balance in sediment exchange with the flood-tidal delta. This balance depends on a prescribed transport from the flood-tidal delta to the inlet and the export of sediment from the inlet to the flood-tidal delta due to tidal currents. We use a simple model for an inlet-bay system, as was derived by Brown (1928) and used by Escoffier (1940) to explain the stability of tidal inlets. The changes on the cross-sectional area of the inlet governed by these dynamics are described by

$$G_{Esc} = -\frac{M}{W_b}\left(1 - \left(\frac{U}{U_e}\right)^2\right) \ . \tag{3}$$

In this equation, W_b is the width of the barrier, U is the amplitude of the tidal current in the inlet (which depends on the imposed tidal range at sea, the cross-sectional area of the inlet, the barrier width, and the wetted surface of the back-barrier lagoon), U_e is the amplitude of the tidal current at equilibrium (set at 1 m/s for all simulations), and M is the volume of sediment per time unit that the inlet receives from the flood tidal delta. With this representation of tidal dynamics we allow for the inlet to evolve toward an equilibrium configuration, using a parametrisation of the net sediment transport due to tides that was earlier used by van de Kreeke (1998, 2004). This evolution differs from the behavior imposed in the BRIE model, were the inlet instantly attained its equilibrium cross-sectional area.

The increase in the cross-sectional area of the inlet due to merging with other inlets is such that the total cross-sectional area is conserved,

$$G_m = \sum_{i=1}^{N_m} \frac{dA_i}{dt} \ . \tag{4}$$

Here, N_m is the number of inlets with which the considered inlet is merging, and A_i are their respective cross-sectional areas.

Lastly, the increase in the cross-sectional area of the inlet due to barrier drowning depends on the length of the portion of the barrier that drowned W_d (either due to negative barrier width or negative barrier height),

$$G_d = \frac{dW_d}{dt}\ \gamma_{aspect}^2 W_d \ , \qquad (5)$$

where the corresponding depth is computed using the inlet aspect ratio γ_{aspect} (with $\gamma_{aspect}^2 = D_{inlet}/W_{inlet}$).

The difference between the BRIE and the BRIE-D models is the temporal evolution of the width of the inlets. In the BRIE model, inlets instantly achieved a width defined by the equilibrium between sediment import by the littoral drift and sediment export by tidal currents. In contrast, the width of inlets in the BRIE-D model gradually adapts depending on the four terms present in Equation 1, and defined in Equations 2 – 5. Given that these differences affect the dynamics of the whole barrier chain, not only inlet widths are different in both models, but also inlet position and number may differ.

2.1.5 Evolution of the Shoreline

The shoreline evolves as a result of divergence of alongshore sediment transport, which is parameterized using the CERC formula and the presence of cross-shore sediment motion. Overwash and inlet dynamics result in a sink of sediment for the shoreline, while shoreface transport may result in a sink or source of sediment, depending on its direction. Following Ashton and Murray (2006), this results in a forced diffusion equation (see Equation 70 of the SI), in which the diffusion coefficient depends on wave characteristics and the orientation of the shoreline.

2.1.6 Initial and Boundary Conditions

Simulations are initialized with a barrier without inlets. The position of the seaward shoreline $x = x_s$ is computed imposing the equilibrium shoreface slope between $x = x_t$ and $x = x_s$ and adding a random perturbation following a uniform distribution between 0 and 1 m. The back-barrier shoreline is set such that the barrier width equals its critical value. The barrier height is also set equal to its critical value. These are representative values for barrier width and height (Leatherman, 1979). We apply periodic boundary conditions in the alongshore direction.

2.1.7 Numerical Aspects

The alongshore extent of the domain covers 50 km with a grid size of 100 m. We solve the equation for the cross-sectional area of the inlet (Equation 1) using an Euler forward scheme with a time step $\Delta t = 0.05$ yr $\sim$ 18 days. The diffusion equation defining the shoreline evolution (Equation 70 of the SI) is solved using a Crank-Nicolson scheme (Crank & Nicolson, 1947).

2.2 Design of Simulations

We run all simulations for 2500 yrs, taking a rate of SLR of $\dot{\xi} = 2$ mm/yr during the first 2000 yrs, which serve as model spin-up. After model spin-up, when the system reaches a statistically stationary state in terms of inlet number and inlet migration rates, we change $\dot{\xi}$ in order to study the system response for another 500 yrs. All other parameters are kept constant during the entire 2500 yrs (see Appendix A for a full overview

Table 1. Overview of simulations performed, imposing different values for the rate of SLR ($\dot{\xi}$) and significant wave height (H_s).

Aim	Model used	Parameter range[a]	Figure
Effects of inlet widening	BRIE, BRIE-D	$\dot{\xi} = 4, 17$ mm/yr	3, 4
Temporal evolution of barrier drowning	BRIE-D	$\dot{\xi} = 4, 17$ mm/yr	5
Dependence on model parameters	BRIE-D	$\dot{\xi}$ varying between 2 and 20 mm/yr, H_s varying between 0.75 and 3 m[b]	6, 7, 8

[a] If not specified parameters take their default values (see Appendix A).
[b] Mulhern et al. (2017)

of the model parameters and their default values). The new $\dot{\xi}$ is not changed during the last 500 yrs of model evolution.

We simulate barrier response to rates of SLR $\dot{\xi}$ between 2 and 20 mm/yr. The following equivalences can be considered at global scale over the next centuries: RCP2.6 and ~ 5 mm/yr, RCP4.5 and ~ 6 mm/yr, RCP8.5 and ~ 10 mm/yr (IPCC, 2021; Palmer et al., 2020). Simulations span a broad range of significant wave heights H_s (between 0.75 and 3 m). Since this is a stochastic system, where randomness originates from the wave angle and from the initial value of x_t, we perform five model realizations for each parameter setting. The default parameter set includes a tidal amplitude of 0.8 m and a wave height of 1.5 m, which are representative values for a typical barrier island system, such as that in the Dutch Wadden Sea. Table 1 presents an overview of the simulations performed.

We investigate the effects of barrier drowning on the widening of inlets by comparing the outcome of the BRIE-D model with that of the BRIE model for low and high $\dot{\xi}$ (4 and 17 mm/yr). We also study the temporal evolution of barrier island drowning for these same two rates of SLR. Moreover, we present the dependence of barrier drowning on a broad range of significant wave height and rates of SLR.

We present the model results as the mean of the five realizations for each parameters setting. Errors are quantified using the standard error of the mean. Experiments performed with an ensemble size of 100 showed no significant differences in model outcome when compared to results computed with only five simulations.

We explored the sensitivity of model output to halving the grid size Δy and halving the time step Δt and found that differences were smaller than 3% for the situation with default parameter values.

2.3 Analysis of Model Output

We quantify barrier drowning by the fraction of the barrier lying below MSL due to tide-wave imbalance in the inlet,

$$\Delta F(t) = F(t) - F_{eq}(t) \ . \tag{6}$$

Here, F and F_{eq} are both fractions of the barrier lying below MSL, computed as sums of the widths of all inlets (a total of $N(t)$) divided by the alongshore extent of the barrier,

$$F(t) = \frac{\sum_{i=1}^{N(t)} W_{inlet,i}(t)}{L_b} \ , \quad F_{eq}(t) = \frac{\sum_{i=1}^{N(t)} W_{inlet,eq,i}(t)}{L_b} \ . \tag{7}$$

Their difference concerns the fact that F_{eq} is calculated by setting the tidal current amplitude in the inlet equal to its equilibrium value ($U_e = 1$ m/s), from which the corresponding equilibrium cross-sectional area is computed (further details are given in SI1). In Equation 7, L_b is the alongshore extent of the barrier, $N(t)$ is the number of inlets at time t, W_{inlet} is the inlet width, and $W_{inlet,eq}$ is the equilibrium inlet width defined by the balance in sediment exchange in the inlet. Thus, ΔF mainly represents the increase of the fraction of the barrier lying below MSL due to the effects of flooding caused by SLR.

Note that F_{eq} is not identical to the F that would be obtained when using the BRIE model. This is because the time evolution of both models is governed by different dynamics, so the number and distribution of inlets will be different in both models.

Increasing SLR does not only affect $\Delta F(t)$, but it may also affect $F_{eq}(t)$. The inlet equilibrium width depends on the tidal prism, among other system characteristics, which can also be affected by SLR. Indeed, an increase in sea level may result in an increase in tidal prism due to a widening of the back-barrier lagoon. Thus, an increase in SLR may induce an increase in the equilibrium inlet width, even if the system is not drowning.

With these definitions for F, F_{eq} and ΔF we are able to quantify the different effects of SLR on barrier systems, from changes in equilibrium width, up to drowning of the barrier due to a decrease in sediment availability.

We define drowning timescales as the time needed for ΔF to take a value of 0.1 or 0.3. We also investigate the evolution of the number of inlets as well as that of barrier width, summarized by its alongshore mean through time. The barrier width is computed as the distance between the seaward shoreline and the back-barrier shoreline $W_b = x_b - x_s$. We compute the barrier width only along the portions corresponding to subaerial barrier, i.e., where $W_b > 0$.

3 Results

3.1 Manifestation of Drowning in BRIE-D Compared to BRIE

An example model simulation under a rate of SLR $\dot{\xi} = 17$ mm/yr shows a gradual expansion of inlets during 500 yrs of barrier evolution (Figure 3). There is a gradual evolution towards a drowned barrier: initially (after the model spin-up period) the barrier has achieved a statistical equilibrium state, after 200 yrs drowning has started, and after 400 yrs more than half of the alongshore extent of the barrier lies below MSL. The transition from a state in which inlets are in morphodynamic equilibrium towards a state of drowning is evident after 200 yrs, as the number of inlets increases and some inlets become much wider than in the equilibrium situation. From there on, some of the inlets merge together until reaching a width of the order of tenths of km by the year 400.

There are differences between the outcomes of the BRIE and the BRIE-D model already at low $\dot{\xi}$ (e.g., 4 mm/yr, see Figure 4a,b), i.e., in situations where the inlets are close to equilibrium and there is no drowning. Inlets tend to close more easily in the BRIE-D model than in the BRIE model as a result of the new sediment dynamics imposed in the inlet. Nevertheless, under these circumstances inlet width remains approximately constant in time in the BRIE-D model, as it is the case with the BRIE model. Furthermore, inlet migration rates are generally similar in both models ($\sim 1-2$ m/yr), with the exception of short periods in which the BRIE-D model yields migration rates of order 200 m/yr, due to local narrowing of the barrier.

The increase in inlet width observed in Figure 3 is the main result of our modifications in the BRIE model. The BRIE model is by definition not able to model situa-

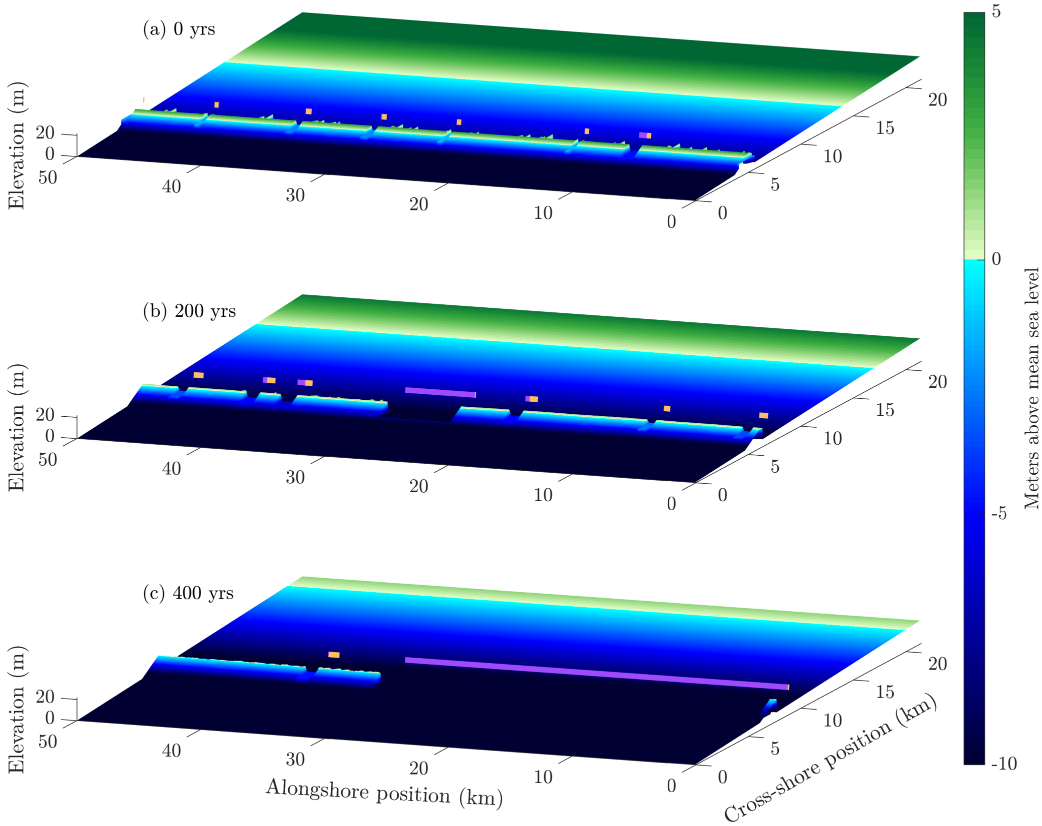

Figure 3. Modeled barrier island evolution at years **(a)** 0, **(b)** 200 and **(c)** 400 after the model spin-up period. Simulation is for $\dot{\xi}$ = 17 mm/yr in order to visualize inlet widening caused by barrier drowning. The number of inlets increases substantially between years 0 and 200, and inlets get wider between years 200 and 400. Orange lines represent the equilibrium inlet width for each inlet ($W_{inlet,eq}$) and purple lines the difference between the actual inlet width an that of equilibrium. Note the differences between actual and equilibrium inlet widths for years 200 and 400. All parameters except $\dot{\xi}$ have their default values (see Table A1); in particular the offshore significant wave height is $H_s = 1.5$ m and the tidal amplitude is $a_0 = 0.8$ m.

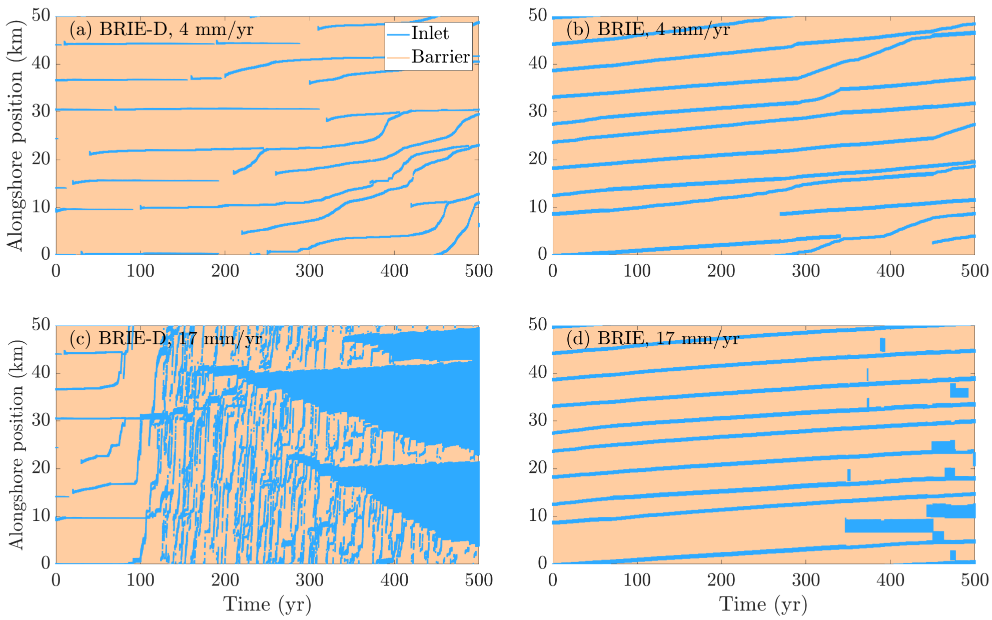

Figure 4. Comparison between the BRIE-D model and the BRIE model: Temporal evolution of barrier systems during 500 yrs in a 50 km long domain for a $\dot{\xi}$ of **(a,b)** 4 mm/yr (barrier drowning is not occurring) and **(c,d)** 17 mm/yr (there is barrier drowning causing widening the inlets). Simulations **(a,c)** were performed using the BRIE-D model, whilst simulations **(b,d)** were performed using the BRIE model. All parameters except $\dot{\xi}$ have their default values (see Table A1); in particular the offshore significant wave height is $H_s = 1.5$ m and the tidal amplitude is $a_0 = 0.8$ m.

tions in which the inlet width gradually increases due to drowning of the barrier. These differences are stressed in Figure 4c,d, for the situation with a high rate of SLR ($\dot{\xi} = 17$ mm/yr). In general, the BRIE model does not always present a continuous evolution of inlet widths, with abrupt changes taking place for example at years 450 or 465, or with inlet closing briefly after opening at years $350 - 400$, yielding unrealistic behavior because of barrier drowning that was unconnected to (other) inlet dynamics. In contrast, with the adaptations implemented in the BRIE-D model in terms of the evolution of the cross-sectional area of the inlet, we are able to account for widening of the inlet due to barrier drowning, yielding a more smooth barrier behavior.

Both models also differ in inlet migration rates, with the BRIE-D model yielding higher migration rates (~ 5 km/yr) than in the BRIE model (~ 10 m/yr) for narrow inlets (< 2 km) in drowning barriers. High migration rates in BRIE-D are due to the barrier being very narrow (< 100 m, see Figure 5b). It is unclear whether this result is realistic. This discrepancy between the two models is caused by the disconnection of the updrift and downdrift barrier tips, imposed to allow for inlet widening beyond its equilibrium state. This disconnection causes differences in sediment deposition in the inlet, which can alter inlet migration.

3.2 Temporal Evolution of Barrier Drowning

The mean fraction of the barrier lying below MSL, F, gradually increases from the year 100 for a situation with a high rate of SLR ($\dot{\xi} = 17$ mm/yr, see Figure 5a) up to

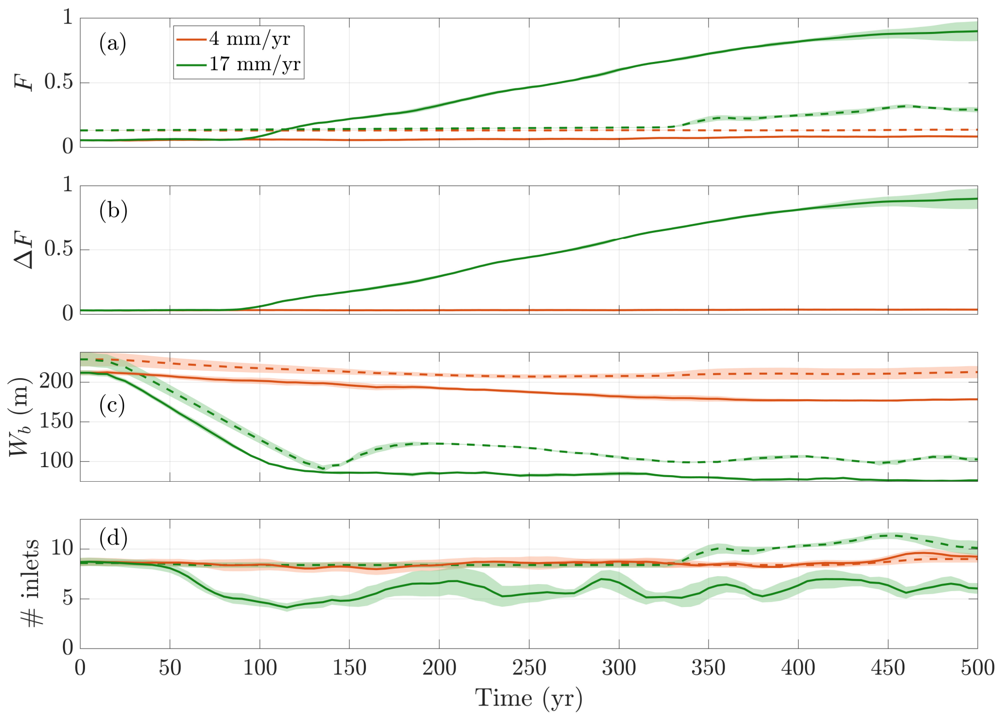

Figure 5. **(a)** Time series of the fraction of the barrier lying below MSL F for $\dot{\xi} = 4$ mm/yr and $\dot{\xi} = 17$ mm/yr, for both the BRIE-D model (solid lines) and the BRIE model (dashed lines). **(b)** As (a), but for the fraction of the barrier lying below MSL due to tide-wave imbalance in the inlet (ΔF) for the BRIE-D model. Note that $\Delta F = 0$ for the BRIE model. **(c)** As (a), but for mean barrier width. **(d)** As (a), but for the number of inlets. Curves represent the mean over five simulations. Shaded areas represent the standard error of the mean, which is very low for some of the variables (e.g., F until year 400). Dashed black lines in panel (b) correspond to the situations depicted in Figure 8 ($\Delta F = 0.1$, 0.3).

~ 0.8 after 500 yrs. Note that the simulation performed with the BRIE model also shows an increase in fraction of the barrier lying below MSL, caused by the increase in tidal prism, reaching values up to $0.3 - 0.4$. This increase in F for the BRIE model corresponds to the sudden inlet creation and inlet widening taking place from the year 350 onward (see Figure 4d). Regarding the BRIE-D model, the temporal evolution of F results from the gradual inlet widening obtained from the year ~ 100 (see Figure 4c). The situation with low rate of SLR ($\dot{\xi} = 4$ mm/yr) shows a constant fraction of the barrier lying below MSL for both models.

In the BRIE-D model, inlet widening due to wave-tide imbalance, ΔF, is the main agent causing the increase in fraction of the barrier lying below MSL (see Figure 5b). The fraction ΔF starts to deviate from zero after 100 yrs of evolution under $\dot{\xi} = 17$ mm/yr, and achieves a value of 0.85 after 400 yrs more. In contrast, the simulation with $\dot{\xi} = 4$ mm/yr never achieves a drowning situation, i.e., ΔF is always close to zero with maximum variations of 0.001. In this situation of low rate of SLR, the barrier is able to adapt to the changes in MSL given that both F and ΔF are kept constant. This means that landward migration of the barrier is effective enough such that the tidal prism is not changed and there is not drowning caused by SLR.

After $\sim$ 110 yrs, the simulation with $\dot{\xi} = 17$ mm/yr attains $\Delta F = 0.1$. At this same stage, the barrier response starts to differ from its previous behavior (see Figure 4c), with inlets becoming notably wider than they were initially.

Barrier width rapidly decreases in the simulations with $\dot{\xi} = 17$ mm/yr during the first $\sim 100-150$ yrs of evolution after spin-up (see Figure 5c). These first 100–150 yrs represent a transition period in which the barrier is accommodating to the new $\dot{\xi}$, which can also be seen in Figure 4c. There is also a minor decrease in barrier width for the case $\dot{\xi} = 4$ mm/yr regardless of the inlets being always close to equilibrium. The barrier width eventually reaches an equilibrium value that depends on the $\dot{\xi}$ imposed. That value is about 30 m larger when using the BRIE model instead of the BRIE-D model for the two values of $\dot{\xi}$ shown. This difference is due to the added inlet dynamics in the BRIE-D with respect to the BRIE model. In particular, we allow for an exchange of sediment between the inlet and the flood-tidal delta in the BRIE-D model, which can reduce or grow the back-barrier.

Both models produce roughly the same number of inlets for $\dot{\xi} = 4$ mm/yr, because the inlets are close to equilibrium, and in those scenarios the number of inlets is controlled solely by the available tidal prism (i.e., $\Delta F \sim 0$). In this situation, inlet number is kept constant at $\sim 8-9$. Substantial differences between the two models arise for the simulations with $\dot{\xi} = 17$ mm/yr. The number of inlets remains constant at around $\sim 8-9$ for the BRIE model, showing no big differences with the situation with lower $\dot{\xi}$ until the year 350. At that time, it increases up to $\sim 11-12$. Note that the barrier behavior for the BRIE simulations with $\dot{\xi} = 17$ mm/yr starts to become irregular from the year 350 as well (see Figure 4d), with inlets closing briefly after opening and sudden changes in inlet width. In contrast, the inlet number decreases up to $\sim 5-6$ with the BRIE-D model and stabilizes around this number from the year ~ 200 onward. The reason that for $\dot{\xi} = 17$ mm/yr there are fewer inlets simulated by the BRIE-D model than by the BRIE model is that inlets are wider, thus there is less subaerial portion of the barrier where inlets can form and survive without merging with other existing inlets.

The change in rate of SLR that the barrier system undergoes at $t = 0$ modifies the barrier response. After this change, the barrier will attain a new statistical equilibrium state. It takes $100-150$ yrs for the barrier to adapt to the new conditions (Figure 5). This time lag in barrier response to variations in the rate of SLR is driven by the gradual evolution imposed in inlet dynamics, which affect the dynamics of the whole barrier chain.

3.3 Wave height and SLR effects on barrier drowning

We performed a sensitivity analysis, as described in Section 2.2. Of the parameters considered, the significant wave height H_s and the rate of SLR $\dot{\xi}$ turned out to be the parameters with the strongest impact on barrier drowning (see Appendix B).

The fraction of the barrier lying below MSL, F, may change due to the variations induced by a new tide-wave balance (dependent on e.g., tidal prism, and wave-driven littoral drift, represented by F_{eq}), and by SLR-induced drowning (which causes tide-wave imbalance, here represented by ΔF). The equilibrium fraction of the barrier lying below MSL, F_{eq}, shows a dependence on significant wave height H_s and rate of SLR $\dot{\xi}$ (see Figure 6a). This dependence is mainly caused by variations in tidal prism and sediment imported by waves. For example, larger significant wave heights cause a decrease in F_{eq} for low rates of SLR, as it is the case for the number of inlets. Nevertheless, the variations in the fraction of the barrier lying below MSL caused by the changes in equilibrium inlet widths are low compared to the effects of drowning (see Figure 6b). Thus, the variations in the total fraction of the barrier lying below MSL, F, are mainly dominated by the tide-wave imbalance in the inlet (i.e., the widening of inlets due to mainly SLR,

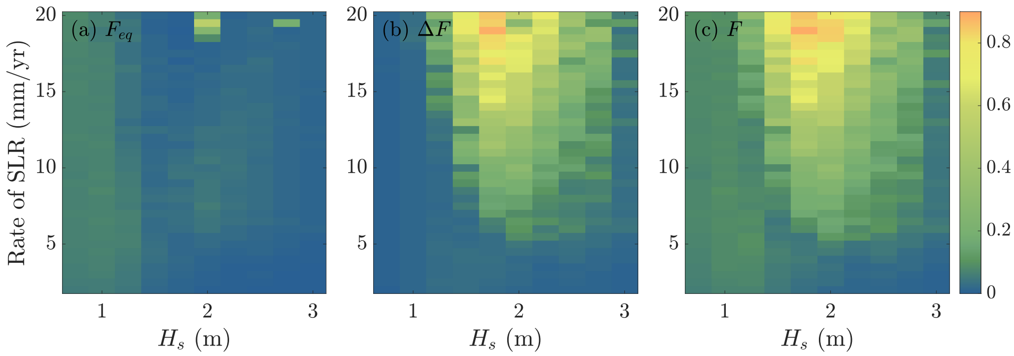

Figure 6. For different values of significant wave height H_s and rate of SLR $\dot{\xi}$: color plots of the **(a)** the fraction of the barrier lying below MSL assuming an equilibrium situation for the inlets (F_{eq}), **(b)** the fraction of the barrier lying below MSL due to tide-wave imbalance in the inlet (ΔF), **(c)** the fraction of the barrier lying below MSL ($F_{eq} + \Delta F = F$) at the year 300.

ΔF). The behavior of F is only dominated by that F_{eq} for low rates of SLR ($\dot{\xi} < 5$ mm/yr), where the effect of SLR is lower (see Figure 6c).

Color plots of fraction of drowned barrier due to wave-tide imbalance ΔF, barrier width W_b and number of inlets as a function of H_s and $\dot{\xi}$ are shown in Figure 7 at years 100, 300 and 500 after the model spin-up period. The situations depicted in white in panels (c2,c3) correspond to simulations that became numerically unstable while inlets were widening due to barrier drowning and thus stopped before reaching the year 500. In some other simulations, the barrier totally drowned before the year 500. For visualization purposes, we have set the barrier width as well as the number of inlets to zero, and ΔF to 0.9 in the latter situations. The quantities shown in all panels are computed as the mean of five simulations.

The general tendency is that an increase in $\dot{\xi}$ causes more drowning, as ΔF eventually takes larger values (see Figure 7a1, b1, c1). The fraction of the barrier lying below MSL due to tide-wave imbalance in the inlet, ΔF, deviates from zero for rates of SLR larger than a certain threshold ($\dot{\xi} \sim 6$ mm/yr). For $\dot{\xi}$ lower than 6 mm/yr, maximum differences in ΔF are 0.04 by the year 500. A similar general tendency can be seen for the barrier width W_b (see Figure 7a2 ,b2, c2), which attains lower values at latter times and at higher $\dot{\xi}$.

The sensitivity of the number of inlets on $\dot{\xi}$ and H_s does not show such a clear pattern as that of ΔF or W_b (see Figure 7a3, b3, c3). Specifically, there are some cases with SLR-driven drowning with a low number of inlets with (some of) them being very wide ($W_{inlet} \sim 10-20$ km), as it is the case for $\dot{\xi} = 17$ mm/yr (see Figures 4c, 5). In other cases with barrier drowning, widths of inlets overall take lower values ($W_{inlet} \sim 1-5$ km). Still, the total fraction below MSL is larger than that at equilibrium, because the number of inlets is very large ($\sim 15-20$). Situations in which there is barrier drowning with a large number of relatively narrow inlets are characterized by high waves ($H_s \geq 2$ m) and rates of sea level rise generally lower than 15 mm/yr. Under these situations, there is an important deposition of sediment by the waves, which creates narrower inlets. In contrast, drowning situations with few and wide inlets only take place for $\dot{\xi} > 15$ mm/yr. In these cases, the combined effect of the deepening of the toe of the shoreface (which depends on the wave height) and sea level rise causes a widening of the inlets which cannot be balanced by the sediment import of waves. Thus, simulations with similar ΔF and W_b may have a significantly different number of inlets. Still, for low $\dot{\xi}$ (such that $\Delta F \sim 0$, i.e., $\dot{\xi} < 5$ mm/yr) the number of inlets decreases significantly for $H_s \geq 2$ m. This

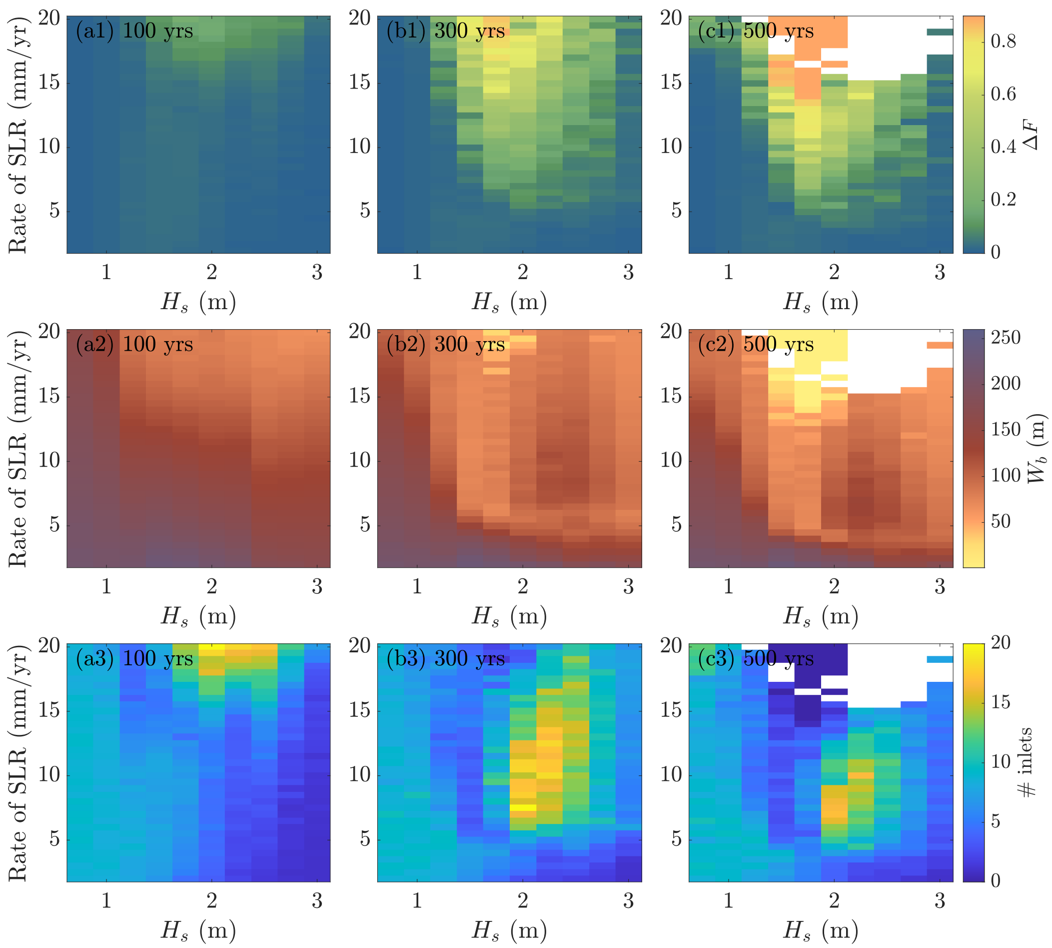

Figure 7. For different values of significant wave height H_s and rate of SLR $\dot{\xi}$: color plots of ΔF **(a1,b1,c1)**, alongshore mean of barrier width W_b **(a2,b2,c2)**, and number of inlets **(a3,b3,c3)**. All three quantities are shown at years 100, 300 and 500 after model spin-up (first, second, and third columns, respectively) and averaged over five simulations.

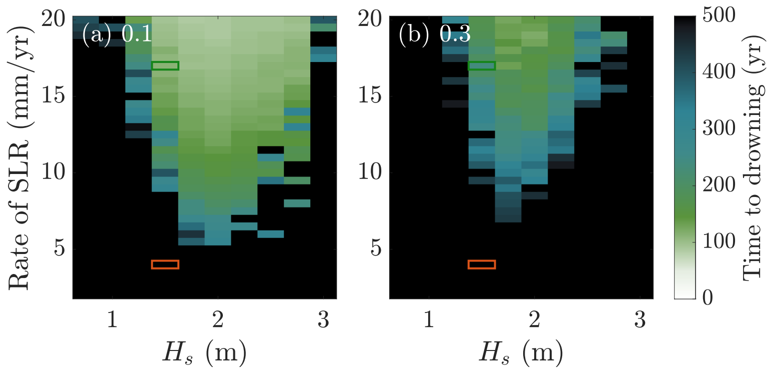

Figure 8. Drowning timescales: time after spin-up needed to increase ΔF by **(a)** 0.1 or by **(b)** 0.3 for different significant wave heights H_s and rate of SLR $\dot{\xi}$. Green and red rectangles refer to the situations shown in Figure 5.

is also because higher waves tend to import more sediment into the inlets, thereby closing them more often when there is no SLR-induced drowning.

Depending on the rate of SLR and on the wave height, the barrier starts drowning (if it does) after a certain time. In all cases, this is not achieved instantly after the rate of SLR changes, but there is a time lag for the barrier system to adapt. Situations in which ΔF attains a value of 0.1 or 0.3 are reached earlier for environments with higher $\dot{\xi}$ and intermediate H_s (Figure 8). The dependence of the time lag on the rate of SLR, arises from the gradual evolution of the inlets cross-sectional area. Still, for the same rate of SLR, this lag in barrier response depends on the wave height as well, with intermediate wave heights ($H_s \sim 2$ m) yielding the fastest barrier response. This is because intermediate H_s cause more drowning due to the deepening of the shoreface toe, which cannot be counteracted by the sediment imported by waves. For highers waves, sediment imported by the littoral drift is able to counteract the effects of the deepening of the shoreface toe, and it takes longer for a barrier to drown. For lower waves, even if the sediment imported by the littoral drift is not so abundant, the toe of the shoreface is shallower, thus the whole barrier system can adapt faster to SLR-induced drowning. Interestingly, even if most situations deviate from equilibrium (Figure 7), not all of them reach a state of $\Delta F = 0.1$ within 500 yrs.

Model simulations of barrier drowning are robust. All quantities shown in Figures 6, 7, 8 have a low standard deviation of the mean compared to their mean values. For ΔF, this value takes generally values below 0.05 and only reaches 0.15 in situations where ΔF is of the order of 0.9. The standard deviation of the mean barrier width is always below 15 m, and generally around 5 m. Lastly, the standard deviation of the mean number of inlets is always below 3.

4 Discussion

4.1 Comparison with Observations and Earlier Models

The cross-shore dynamics reproduced with the BRIE-D model are similar to those obtained by the BRIE model of Nienhuis and Lorenzo-Trueba (2019b) or an earlier 2D horizontal barrier island model (which did not include inlets) of Lorenzo-Trueba and Ashton (2014). For example, the width of the subaerial portion of the barrier eventually attains a constant value that depends on the rate of SLR $\dot{\xi}$. Lorenzo-Trueba and Ashton (2014) found the same behavior and termed this state as dynamic equilibrium, because the barrier is still migrating landward, but its width does not change. Similarly, the increase in barrier drowning found for larger wave heights due to a deepening of the toe of the shoreface is in agreement with results of Lorenzo-Trueba and Ashton (2014). Differences include the maximum barrier transgression rate, which can be higher in BRIE and BRIE-D, because these also account for sources and sinks of sediment in the barrier due to inlet and alongshore dynamics.

Compared to BRIE, the BRIE-D model computes very high inlet migration rates when rates of SLR are higher ($\sim$ 5 km/yr, see Figure 4c). Barrier narrowing due to SLR may increase inlet migration rates. However, a compilation of observed inlet migration rates shows they are notably lower (e.g., highest observed rate is 700 m/yr, Nienhuis & Ashton, 2016) than the values obtained with the BRIE-D model. The BRIE model yields more realistic migration rates (of the order of 10 m/yr, see Figure 4d). These differences are caused by the new dynamics in alongshore sediment transport deposition within the inlet implemented in the BRIE-D model (first term on the right-hand side of Equation 1). These new dynamics allow for a disconnection of the updrift and downdrift tips of the barrier, and thus inlet widening. However, they also result in, perhaps, unrealistically large inlet migration rates. Inlet dynamics in BRIE-D are based on Delft3D simulations from Nienhuis and Ashton (2016), who computed the distribution of sediment transport between the updrift and downdrift tips of the barrier. However, their experiments were performed with barrier widths between 250 m and 800 m and inlet widths lower than 1 km. Thus, situations with SLR-driven drowning were not included. Future studies should investigate how to better parameterize inlet sediment distributions under drowning situations in which the barrier becomes narrower, possibly inducing new inlet dynamics.

Observations of landward barrier migration back up our results, for example the Isles Dernières in Louisiana have been migrating landward at a rate of $\sim$ 10 m/yr, under a rate of relative SLR of 13 mm/yr (Dingler & Reiss, 1990; Dingler et al., 1993). The BRIE-D model yields a landward migration of the order of $2-8$ m/yr for rates of SLR between 2 and 20 mm/yr. These agreements are expected on longer timescales because barriers then follow the basement slopes, which are O(10^3) m/m.

We obtained good agreement with observations in terms of widening of inlets caused by barrier drowning. For example, the Isles Dernières have experienced gradual drowning during the last 200 yrs, in which $\sim$ 0.7 of their subaerial area has been lost under a rate of relative SLR of 13 mm/yr (Dingler et al., 1993; Davis Jr. & FitzGerald, 2010). These rates are not uncommon. Simulations performed with the BRIE-D model with a rate of SLR of 17 mm/yr resulted in a 0.7 increase in F in 300 years, although under a higher rate of SLR than that measured in the Isles Dernières. There could be other mechanisms inducing a significant land loss in the Isles Dernières, such as marsh drowning, which are not implemented in the BRIE-D model. These comparisons are challenging because of model sensitivities to other factors (e.g., shoreface response rate, maximum overwash fluxes) that are difficult to retrieve from field observations.

Other ways to compare BRIE-D model results with observations include the fraction below MSL, F. In an environment representative of the Wadden Islands (i.e., $\dot{\xi} =$ 4 mm/yr, $H_s = 1.5$ m), the BRIE-D model yields a constant fraction of the barrier lying below MSL of $\sim$ 0.1. This is lower than the observed F of 0.22 (see Figure 1). Not all model parameters have been calibrated for the Wadden Islands, such as marsh cover or wave asymmetry, among others. Nevertheless, for higher rates of SLR ($\dot{\xi} > 18$ mm/yr), the BRIE-D model yields an increase in fraction of the barrier lying below MSL up to 0.6, as SLR-driven inlet widening will dominate the barrier island evolution (see Figure 6).

The BRIE-D model is not able to reproduce all the dynamics involved in barrier drowning. For example, we have not modeled the curvature of barrier tips occurring in wide inlets when bypassing diminishes (Davis Jr. & FitzGerald, 2010). Future research should focus on finding appropriate parametrisations for these dynamics and implementing them in the BRIE-D model such that the drowning state of a barrier is modeled as realistically as possible.

Furthermore, the ebb-tidal delta is not explicitly included in the BRIE-D model albeit it is a prominent entity in the sand balance of tidal inlets. Nevertheless, its effects on inlet migration rate and the size of the flood-tidal delta are implicitly taken into account through its effects on waves and currents (Nienhuis & Ashton, 2016). In that sense, the BRIE-D model, as well as the BRIE model, offers a different picture on inlet and barrier dynamics than that in previous studies, such as van de Kreeke (2006).

Still, the BRIE-D model is a reasonable tool to understand the different mechanisms involved in barrier island evolution and, particularly, drowning. Specifically, the multiple parametrisations used in the model make it very computationally efficient, allowing for an in-depth study of the effects of multiple parameters on the response of barrier systems. More observations are needed to properly evaluate and compare projections from BRIE-D, also in comparison with more process-based models such as Mariotti (2021).

4.2 Choice of Parameters

The main objective of this study was to gain insight on the different dynamics related to barrier drowning rather than mimicking real situations. We have thereby kept wave height, tidal range and storm return period constant through the simulations, albeit they are expected to change as $\dot{\xi}$ increases (Bricheno & Wolf, 2018; Pickering et al., 2012). Yet, we have selected their values such that different barrier systems in the world are represented by our simulations (Mulhern et al., 2017; Nienhuis & van de Wal, 2021).

Furthermore, global projections of SLR may not be representative of barrier systems, given the high subsidence rates present in deltas. Consequently, we have chosen constant $\dot{\xi}$ through all simulations. We can thus have a broader range of scenarios and we can apply them in longer-term situations. The only drawback of applying constant rates of SLR is the abrupt change that the system experiences between the spin-up period and the rest of the simulation, which causes an adaptation period of ~ 100 yrs (see Figures 4, 5). Nevertheless, these 100 yrs of adaptation do not seem to alter the gradual path toward drowning of the barriers. Similarly, Mariotti and Hein (2022) found a lag of hundreds of years in barrier response to abrupt changes in rates of SLR. Another consequence of the abrupt change in rate of SLR are the irregularities in the backbarrier shoreline of the barrier just after spin-up (see Figure 3a). Still, these irregularities are smoothed with time and end up disappearing, hence we do not consider them to be a sign of model instability.

Simulations performed with an increasing rate of SLR (based on RCP scenarios) showed the same tendency as the respective simulations with equivalent constant rates of SLR (i.e., RCP2.6 and $\dot{\xi} = 5$ mm/yr, RCP4.5 and $\dot{\xi} = 6$ mm/yr, RCP8.5 and $\dot{\xi} = 10$ mm/yr; see Figure S8). Future studies could, however, study in further detail the effects of a gradual increase in rate of SLR by varying the increase in sea level as well as the timescale involved in this gradual evolution.

5 Conclusions

Here we aimed to (1) understand how the fraction of the barrier lying below MSL is affected by SLR, (2) examine the temporal evolution of the barrier island drowning, as well as quantifying drowning timescales, and (3) explore its dependence on model parameters. With our new model (BRIE-D), we have performed simulations with a wide range of values for significant wave height H_s and rate of SLR $\dot{\xi}$. Using the model output, we have quantified barrier island drowning by computing the total fraction of the barrier lying below MSL F, that caused by tide-wave imbalance ΔF, the alongshore mean of the barrier width, and the number of inlets.

Effects of SLR on barrier islands manifest as an increase of inlet width and/or an increase in inlet number. Barriers drown faster for higher $\dot{\xi}$. Barrier response to changes in rates of SLR takes place at timescales of the order of hundreds of years, and occurs in a gradual manner. It takes $\sim$ 100 yrs for a barrier to adapt to a different rate of SLR. After this period, drowning may occur under high rates of SLR within the following centuries.

We expect environments with intermediate wave heights ($\sim$ 2 m) to be most sensitive to SLR-induced drowning. Lower wave environments have shallower depth of closure and can respond faster to SLR. Higher waves trigger two opposed mechanisms: a more frequent inlet closure, and a more intense barrier drowning. The former is caused by the larger amount of sediment imported into the inlet system, whereas the latter is a result of the deeper shoreface toe, which makes a barrier system more prone to drowning.

Appendix A Default model parameters

Unless stated otherwise model parameters take their default values, given in Table A1.

Table A1. Default values of model parameters. Shortened references are as follows: LTA14 (Lorenzo-Trueba & Ashton, 2014), B80 (Bowen, 1980), M17 (Mulhern et al., 2017), AM06 (Ashton & Murray, 2006), SZ09 (de Swart & Zimmerman, 2009), R13 (Roos et al., 2013), N15 (Nienhuis et al., 2015).

Name	Value	Units	Explanation
ρ_w	1025	kg m^{-3}	Density of water
ω	$1.4 \cdot 10^{-4}$	s^{-1}	Offshore tidal radial frequency
g	9.81	m s^{-2}	Gravitational acceleration
R	1.65	–	Submerged specific gravity of sediment
e_s	0.01	–	Suspended sediment transport efficiency factor (LTA14)
c_s	0.01	–	Friction factor (B80)
n	0.05	s m$^{-1/3}$	Manning roughness coefficient
$\dot{\xi}$	10	m yr^{-1}	Rate of SLR
H_s	1.5	m	Significant wave height in deepwater (M17)
a_0	0.8	m	Offshore tidal amplitude (M17)
T_{storm}	10	yr	Minimum period between inlet forming storms
T_p	10	s	Peak wave period
a	0.8	–	Wave asymmetry (AM06)
h	0.2	–	Wave highness (AM06)
γ_{aspect}	0.0707	–	Inlet aspect ratio ($\gamma_{aspect}^2 = D_{inlet}/W_{inlet}$)
u_e	1	m/s	Tidal inlet equilibrium velocity (SZ09)
H_{crit}	2	m	Critical barrier height (LTA14)
$W_{b,crit}$	200	m	Critical barrier width (LTA14)
$Q_{ow,max}$	50	m^3 m^{-1} yr^{-1}	Maximum overwash flux (LTA14)
L_{min}	5	km	Minimum distance between tidal inlets (R13)
$s_{background}$	10^{-3}	–	Background slope (LTA14)
k	0.06	m$^{3/5}$ s$^{-6/5}$	Alongshore sediment transport constant (N15)
Δy	100	m	Alongshore grid spacing
Δt	0.05	yr	Time step

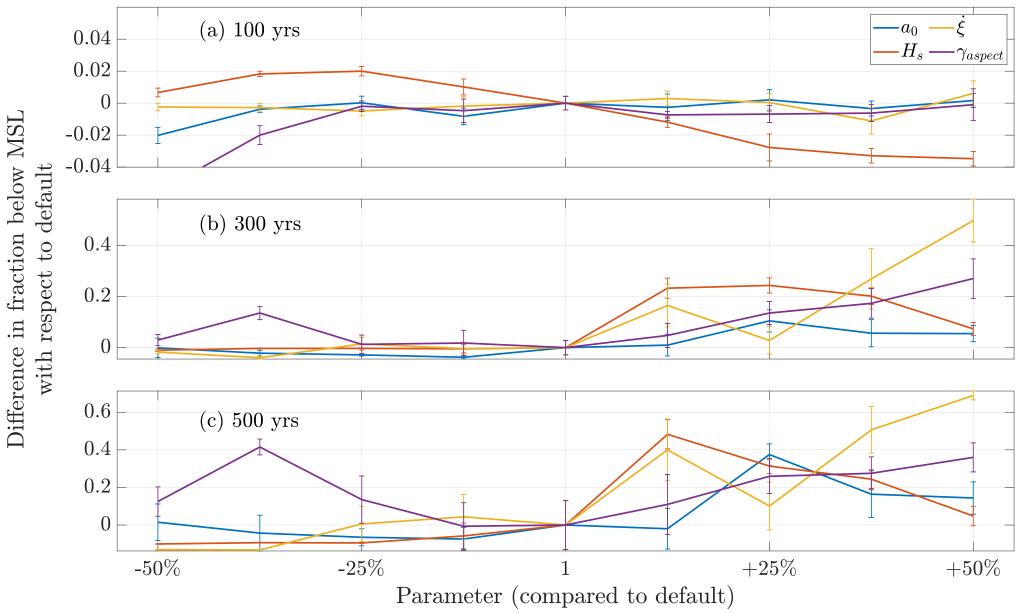

Figure B1. Differences in fraction below MSL with respect to the default case when varying different morphodynamic parameters at **(a)** 100 yrs, **(b)** 300 yrs and **(c)** 500 yrs after model spin up. Note the different scales in the vertical axis.

Appendix B Sensitivity analysis

We performed a sensitivity analysis for the main parameters that control the system: tidal range a_0, significant wave height H_s, wave period T_p, rate of SLR $\dot{\xi}$, wave asymmetry a, inlet aspect ratio γ_{aspect}, maximum overwash transport $Q_{ow,max}$ and the suspended sediment transport efficiency factor e_s, which controls the shoreface transport. We varied each of the parameters around $\pm 50\%$ of their default values and computed the alongshore fraction below MSL at three different stages: at years 100, 300 and 500 after model spin-up. For each set of parameters we created five realizations, from which we computed the mean fraction below MSL and the standard error of the mean. We found clear patterns and deviations from the default case for only four of the eight parameters: a_0, H_s, $\dot{\xi}$ and γ_{aspect} (see Figure B1). Among these four, largest variations were observed for the significant wave height H_s and the rate of SLR $\dot{\xi}$. Thus, we decided to study the dependence of the model on these parameters in more detail (see Section 3.3).

Increasing the tidal range, a_0, results in a generally larger fraction below MSL due to a gain in tidal prism, which increases the amount of sediment exported by tidal currents (de Swart & Zimmerman, 2009). Lower tidal ranges cause a lower fraction below MSL F due to less sediment being exported by tidal currents.

Regarding the significant wave height, we observe two opposite behaviors in terms of F. Depending on the time after model spin-up, higher waves may produce a decrease or an increase in F. This is explained by distinguishing two processes caused by high waves: (1) higher waves tend to import more sediment into an inlet, thereby favoring its closure (Escoffier, 1940), and (2) higher waves affect the sediment at deeper bed levels, causing a larger depth of closure (Houston, 1995). A larger depth of closure means that a larger volume of sand responds to sea level variations, yielding a system that is more prone to drowning. After 100 yrs, an increase in significant wave height causes a decrease in fraction below MSL of up to -0.03, while a decrease in H_s increases the fraction below

MSL up to +0.02. This is because at this stage the first mechanism dominates. Nevertheless, after 300 or 500 yrs of model evolution, when the effects of SLR-induced drowning are more prevalent, a decrease in H_s causes a decrease in the fraction of the barrier lying below MSL. On the other hand, there is a larger fraction of the barrier lying below MSL (up to +0.5) for slightly larger H_s (+25%). With higher waves (+50%) the fraction corresponds to 0.5 after 500 yrs. The peak in F attained when increasing H_s by -25% is due to the second mechanism dominating the barrier evolution. The decrease in F (even if still higher than in the default situation) when increasing H_s by +50% is because the first process is more important than in situations with lower waves. The effects of the deepening of the shoreface toe are only visible from year 300 onwards, because the barrier system needs time to adapt and to be affected by SLR.

Increasing the rate of SLR results in more drowning, inducing a fraction below MSL of up to +0.68 by the year 500 for the most extreme case. Note that as explained for significant wave heights, effects of drowning are only visible from year 300 onwards. In contrast, decreasing the rate of SLR decreases the fraction of the barrier lying below MSL up to -0.13 because there is less drowning.

An increase in inlet aspect ratio creates narrower inlets for the same cross-sectional area, thereby yielding a slightly lower fraction below MSL at year 100 (up to -0.01). However, in the years 300 and 500 an increase in inlet aspect ratio results in the opposite effect, yielding an increase in F of up to +0.36. Lowering the inlet aspect ratio makes shallower inlets, increasing the bottom friction. This causes the inlets to be more susceptible to closing, decreasing thus the fraction of the barrier lying below MSL at the year 100 up to -0.05. However, at 300 or 500 yrs after model spin-up, F increases for lower values of the inlet aspect ratio. These differences in behavior between earlier and latter times suggest that the dependence of the barrier evolution on the inlet aspect ratio is susceptible to SLR-driven drowning, similarly to the situation obtained when varying H_s.

Open Research

The code for the BRIE-D model is accessible from `https://doi.org/10.5281/zenodo.7353693`.

References

Ashton, A. D., & Lorenzo-Trueba, J. (2018). Morphodynamics of barrier response to sea-level rise. In L. J. Moore & A. B. Murray (Eds.), *Barrier Dynamics and Response to Changing Climate* (pp. 277–304). Cham: Springer International Publishing. doi: 10.1007/978-3-319-68086-6_9

Ashton, A. D., & Murray, A. B. (2006). High-angle wave instability and emergent shoreline shapes: 1. Modeling of sand waves, flying spits, and capes. *Journal of Geophysical Research: Earth Surface*, *111*(F4). doi: 10.1029/2005JF000422

Beets, D. J., & van der Spek, A. J. F. (2000). The Holocene evolution of the barrier and the back-barrier basins of Belgium and the Netherlands as a function of late Weichselian morphology, relative sea-level rise and sediment supply. *Netherlands Journal of Geosciences - Geologie en Mijnbouw*, *79*(1), 3–16. doi: 10.1017/S0016774600021533

Bowen, A. (1980). Simple models of nearshore sedimentation: Beach profiles and longshore bars. In S. B. McCann (Ed.), *The Coastline of Canada* (Vol. 80-10, p. 1-11). Geological Survey of Canada.

Bricheno, L. M., & Wolf, J. (2018). Future wave conditions of Europe, in response to high-end climate change scenarios. *Journal of Geophysical Research: Oceans*, *123*(12), 8762-8791. doi: 10.1029/2018JC013866

Brown, E. I. (1928). Inlets on sandy coasts. In *Proceedings of the American Society of Civil Engineers* (Vol. 54, pp. 505–554).

Cowell, P., Roy, P., & Jones, R. (1992). Shoreface translation model: computer simulation of coastal-sand-body response to sea level rise. *Mathematics and Computers in Simulation*, *33*, 603–608.

Crank, J., & Nicolson, P. (1947). A practical method for numerical evaluation of solutions of partial differential equations of the heat-conduction type. *Mathematical Proceedings of the Cambridge Philosophical Society*, *43*(1), 50–67.

Davis Jr., R. A., & FitzGerald, D. M. (2010). *Beaches and Coasts*. Wiley.

de Swart, H., & Zimmerman, J. (2009). Morphodynamics of tidal inlet systems. *Annual Review of Fluid Mechanics*, *41*(1), 203-229. doi: 10.1146/annurev.fluid.010908.165159

Dingler, J. R., & Reiss, T. E. (1990). Cold-front driven storm erosion and overwash in the central part of the Isles Dernières, a Louisiana barrier-island arc. *Marine Geology*, *91*(3), 195–206.

Dingler, J. R., Reiss, T. E., & Plant, N. G. (1993). Erosional patterns of the Isles Dernières, Louisiana, in relation to meteorological influences. *Journal of Coastal Research*, 112–125.

Escoffier, F. (1940). The stability of tidal inlets. *Shore and Beach*(8), 114-115.

FitzGerald, D. M., Buynevich, I., & Argow, B. (2006). Model of tidal inlet and barrier island dynamics in a regime of accelerated sea level rise. *Journal of Coastal Research*, 789–795.

FitzGerald, D. M., Fenster, M. S., Argow, B. A., & Buynevich, I. V. (2008). Coastal impacts due to sea-level rise. *Annual Review of Earth and Planetary Sciences*, *36*(1), 601-647. doi: 10.1146/annurev.earth.35.031306.140139

FitzGerald, D. M., J. Hein, C., Hughes, Z., Kulp, M., Georgiou, I., & Miner, M. (2018). Runaway barrier island transgression concept: Global case studies. In L. J. Moore & A. B. Murray (Eds.), *Barrier Dynamics and Response to Changing Climate* (pp. 3–56). Cham: Springer International Publishing. doi: 10.1007/978-3-319-68086-6_1

Gilbert, G. K. (1885). The topographic features of lake shores. In *United States Geological Survey Annual Report* (pp. 69–123).

Houston, J. (1995). Beach-fill volume required to produce specified dry beach width. In *Coastal Engineering Technical Note* (p. 11-32). US Army Engineer Waterways Experiment Station Vicksburg, Mississippi.

IPCC. (2021). Summary for policymakers [Book Section]. In V. Masson-Delmotte et al. (Eds.), *Climate Change 2021: The Physical Science Basis. Contribution of Working Group I to the Sixth Assessment Report of the Intergovernmental Panel on Climate Change* (chap. SPM). Cambridge University Press.

Jiménez, J. A., & Sánchez-Arcilla, A. (2004). A long-term (decadal scale) evolution model for microtidal barrier systems. *Coastal Engineering*, *51*(8), 749-764. (Coastal Morphodynamic Modeling) doi: 10.1016/j.coastaleng.2004.07.007

Leatherman, S. P. (1979). Migration of Assateague Island, Maryland, by inlet and overwash processes. *Geology*, *7*(2), 104-107. doi: 10.1130/0091-7613(1979)7⟨104:MOAIMB⟩2.0.CO;2

Leatherman, S. P. (1983). Barrier dynamics and landward migration with Holocene sea-level rise. *Nature*, *301*(5899), 415–417.

Lorenzo-Trueba, J., & Ashton, A. D. (2014). Rollover, drowning, and discontinuous retreat: Distinct modes of barrier response to sea-level rise arising from a simple morphodynamic model. *Journal of Geophysical Research: Earth Surface*, *119*(4), 779-801. doi: 10.1002/2013JF002941

Mariotti, G. (2021). Self-organization of coastal barrier systems during the Holocene. *Journal of Geophysical Research: Earth Surface*, *126*(5), e2020JF005867. doi: 10.1029/2020JF005867

Mariotti, G., & Hein, C. J. (2022). Lag in response of coastal barrier-island retreat to sea-level rise. *Nature Geoscience*, *15*(8), 633–638. doi: 10.1038/s41561-022-00980-9

Masetti, R., Fagherazzi, S., & Montanari, A. (2008). Application of a barrier island translation model to the millennial-scale evolution of Sand Key, Florida. *Continental Shelf Research*, *28*(9), 1116-1126. doi: 10.1016/j.csr.2008.02.021

Mellett, C. L., & Plater, A. J. (2018). Drowned barriers as archives of coastal-response to sea-level rise. In L. J. Moore & A. B. Murray (Eds.), *Barrier Dynamics and Response to Changing Climate* (pp. 57–89). Cham: Springer International Publishing. doi: 10.1007/978-3-319-68086-6_2

Mulhern, J. S., Johnson, C. L., & Martin, J. M. (2017). Is barrier island morphology a function of tidal and wave regime? *Marine Geology*, *387*, 74-84. doi: 10.1016/j.margeo.2017.02.016

Nienhuis, J. H., & Ashton, A. D. (2016). Mechanics and rates of tidal inlet migration: Modeling and application to natural examples. *Journal of Geophysical Research: Earth Surface*, *121*(11), 2118-2139. doi: 10.1002/2016JF004035

Nienhuis, J. H., Ashton, A. D., & Giosan, L. (2015). What makes a delta wave-dominated? *Geology*, *43*(6), 511-514. doi: 10.1130/G36518.1

Nienhuis, J. H., & Lorenzo-Trueba, J. (2019a). Can barrier islands survive sea-level rise? Quantifying the relative role of tidal inlets and overwash deposition. *Geophysical Research Letters*, *46*(24), 14613-14621. doi: 10.1029/2019GL085524

Nienhuis, J. H., & Lorenzo-Trueba, J. (2019b). Simulating barrier island response to sea level rise with the barrier island and inlet environment (BRIE) model v1.0. *Geoscientific Model Development*, *12*(9), 4013–4030. doi: 10.5194/gmd-12-4013-2019

Nienhuis, J. H., & van de Wal, R. S. W. (2021). Projections of global delta land loss from sea-level rise in the 21st century. *Geophysical Research Letters*, *48*(14). doi: 10.1029/2021GL093368

Ortiz, A. C., & Ashton, A. D. (2016). Exploring shoreface dynamics and a mechanistic explanation for a morphodynamic depth of closure. *Journal of Geophysical Research: Earth Surface*, *121*(2), 442-464. doi: 10.1002/2015JF003699

Palmer, M. D., Gregory, J. M., Bagge, M., Calvert, D., Hagedoorn, J. M., Howard, T., ... Spada, G. (2020). Exploring the drivers of global and local sea-level change over the 21st century and beyond. *Earth's Future*, *8*(9). doi: 10.1029/2019EF001413

Pickering, M., Wells, N., Horsburgh, K., & Green, J. (2012). The impact of future sea-level rise on the European Shelf tides. *Continental Shelf Research*, *35*, 1-15. doi: 10.1016/j.csr.2011.11.011

Reef, K. R. G., Roos, P. C., Andringa, T. E., Dastgheib, A., & Hulscher, S. J. M. H. (2020). The impact of storm-induced breaches on barrier coast systems subject to climate change—A stochastic modelling study. *Journal of Marine Science and Engineering*, *8*(4), 271. doi: 10.3390/jmse8040271

Roos, P. C., Schuttelaars, H. M., & Brouwer, R. L. (2013). Observations of barrier island length explained using an exploratory morphodynamic model. *Geophysical Research Letters*, *40*(16), 4338–4343. doi: 10.1002/grl.50843

Sanders, J. E., & Kumar, N. (1975). Evidence of shoreface retreat and in-place "drowning" during Holocene submergence of barriers, shelf off Fire Island, New York. *Geol. Soc. Am. Bull.*, *86*(1), 65–76.

Storms, J. E., Weltje, G. J., Van Dijke, J., Geel, C., & Kroonenberg, S. (2002). Process-response modeling of wave-dominated coastal systems: simulating evolution and stratigraphy on geological timescales. *Journal of Sedimentary Research*, *72*(2), 226–239.

van de Kreeke, J. (1998). Adaptation of the Frisian Inlet to a reduction in basin area with special reference to the cross-sectional area of the inlet channel. In J. Dronkers & M. Scheffers (Eds.), *Physics of Estuaries and Coastal Seas* (pp. 355–362). Balkema, Rotterdam.

van de Kreeke, J. (2004). Equilibrium and cross-sectional stability of tidal inlets: application to the Frisian Inlet before and after basin reduction. *Coastal Engineering*, *51*(5), 337-350. doi: 10.1016/j.coastaleng.2004.05.002
van de Kreeke, J. (2006). An aggregate model for the adaptation of the morphology and sand bypassing after basin reduction of the Frisian Inlet. *Coastal Engineering*, *53*(2), 255-263. doi: j.coastaleng.2005.10.013

Figure 1.

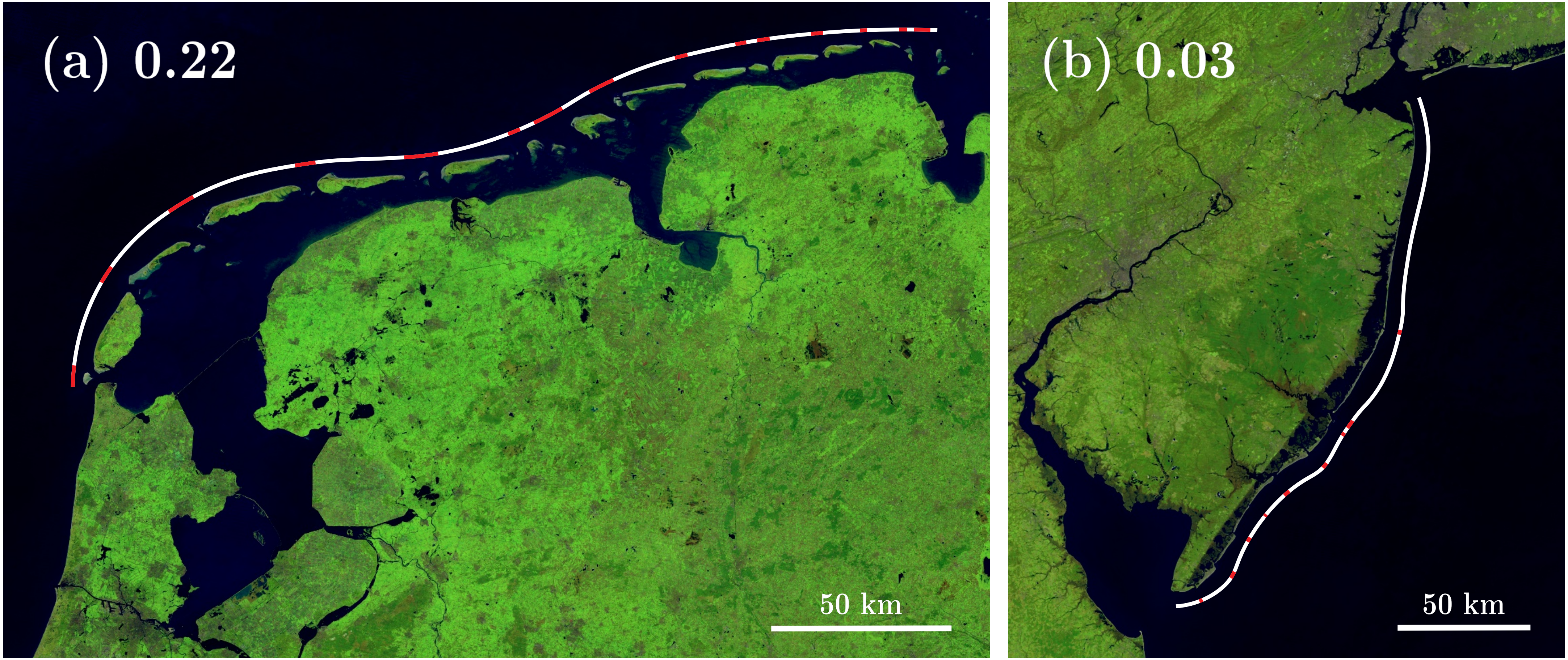
(a) 0.22
50 km
(b) 0.03
50 km

Figure 2.

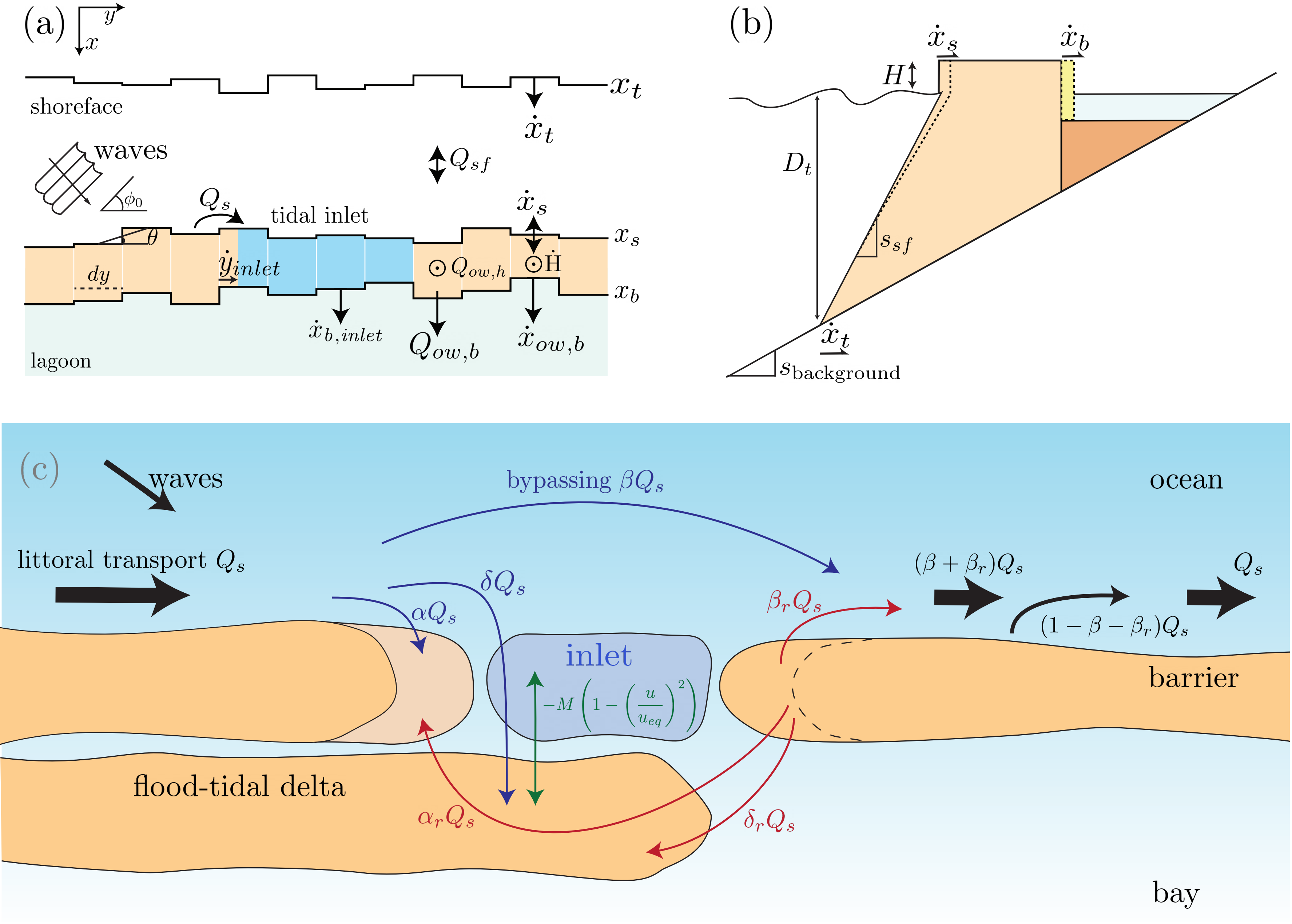

(a)
y
x
x_t
shoreface
$\dot{x}_t$
waves
ϕ_0
Q_{sf}
Q_s
tidal inlet
$\dot{x}_s$
θ
x_s
dy
$\dot{y}_{inlet}$
$\odot Q_{ow,h}$
$\odot \dot{H}$
x_b
$\dot{x}_{b,inlet}$
$Q_{ow,b}$
$\dot{x}_{ow,b}$
lagoon
(b)
$\dot{x}_s$
$\dot{x}_b$
H
D_t
s_{sf}
$\dot{x}_t$
$s_{\mathrm{background}}$
(c)
waves
bypassing βQ_s
ocean
littoral transport Q_s
δQ_s
$(\beta + \beta_r)Q_s$
Q_s
αQ_s
$\beta_r Q_s$
$(1 - \beta - \beta_r)Q_s$
inlet
$-M\left(1 - \left(\frac{u}{u_{eq}}\right)^2\right)$
barrier
flood-tidal delta
$\alpha_r Q_s$
$\delta_r Q_s$
bay

Figure 3.

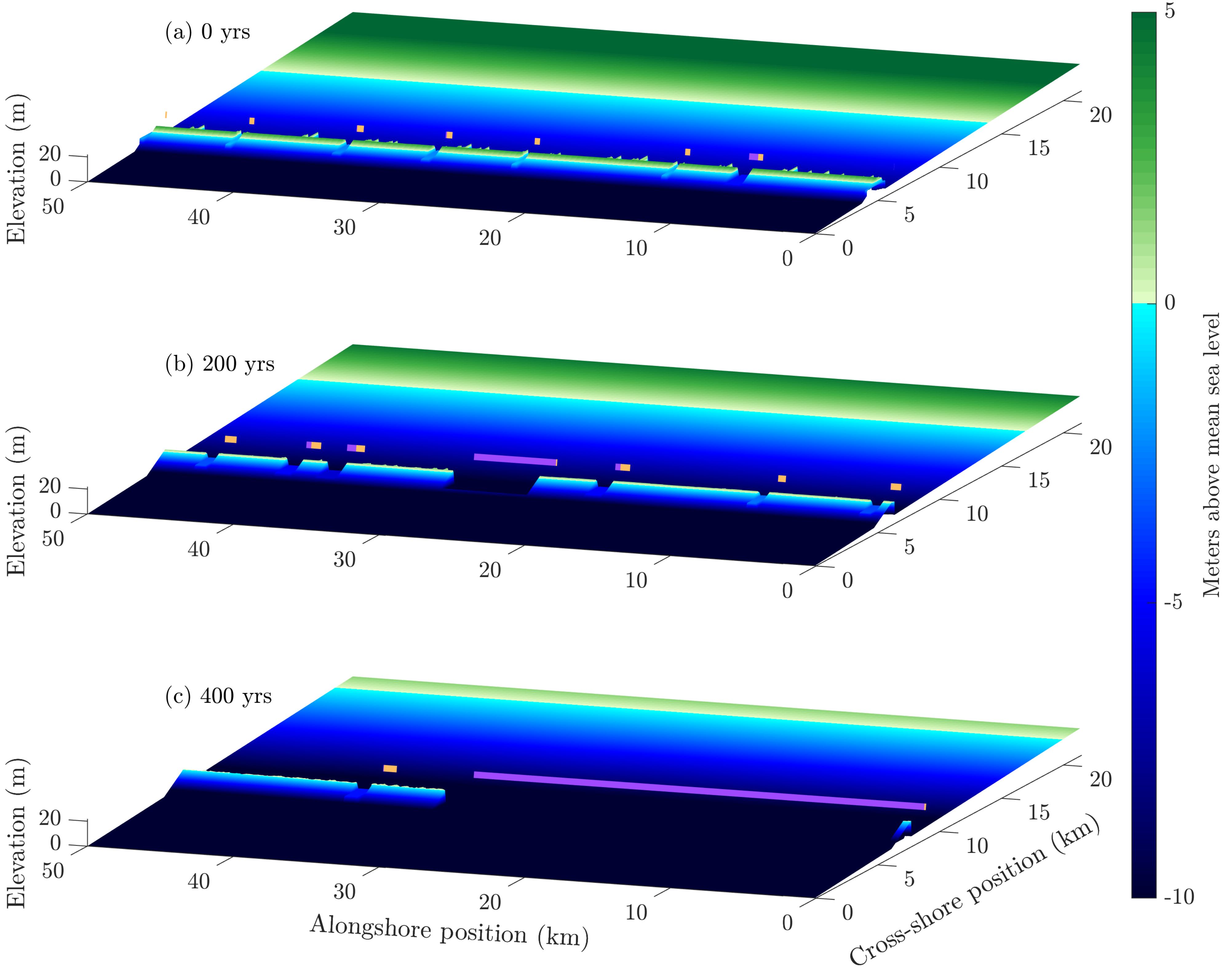
(a) 0 yrs
(b) 200 yrs
(c) 400 yrs
Elevation (m)
Alongshore position (km)
Cross-shore position (km)
Meters above mean sea level

Figure 4.

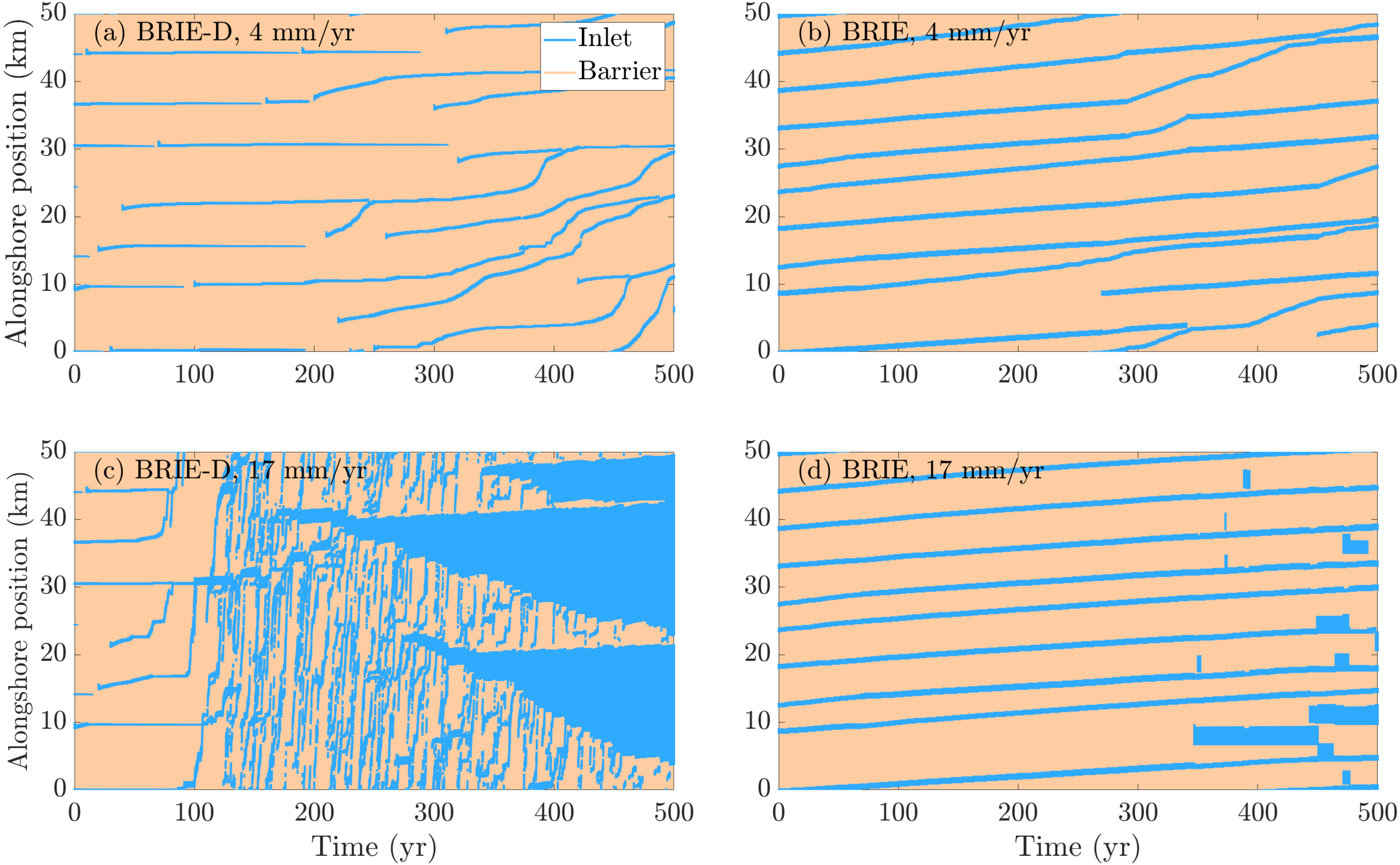

(a) BRIE-D, 4 mm/yr
Inlet
Barrier
(b) BRIE, 4 mm/yr
(c) BRIE-D, 17 mm/yr
(d) BRIE, 17 mm/yr
Alongshore position (km)
Time (yr)
0
10
20
30
40
50
0
100
200
300
400
500

Figure 5.

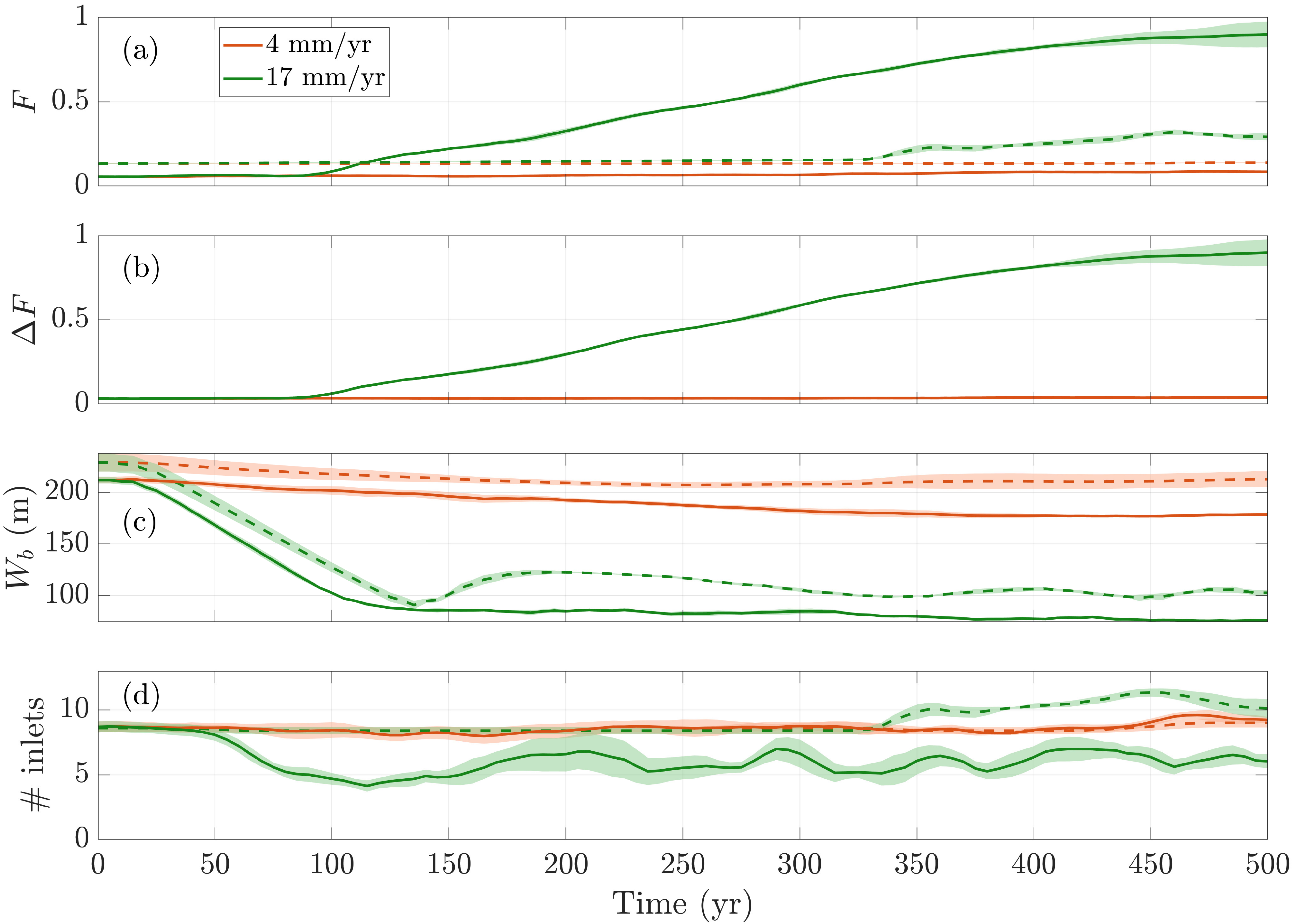
(a)
4 mm/yr
17 mm/yr
F
(b)
ΔF
(c)
W_b (m)
(d)
inlets
Time (yr)

Figure 6.

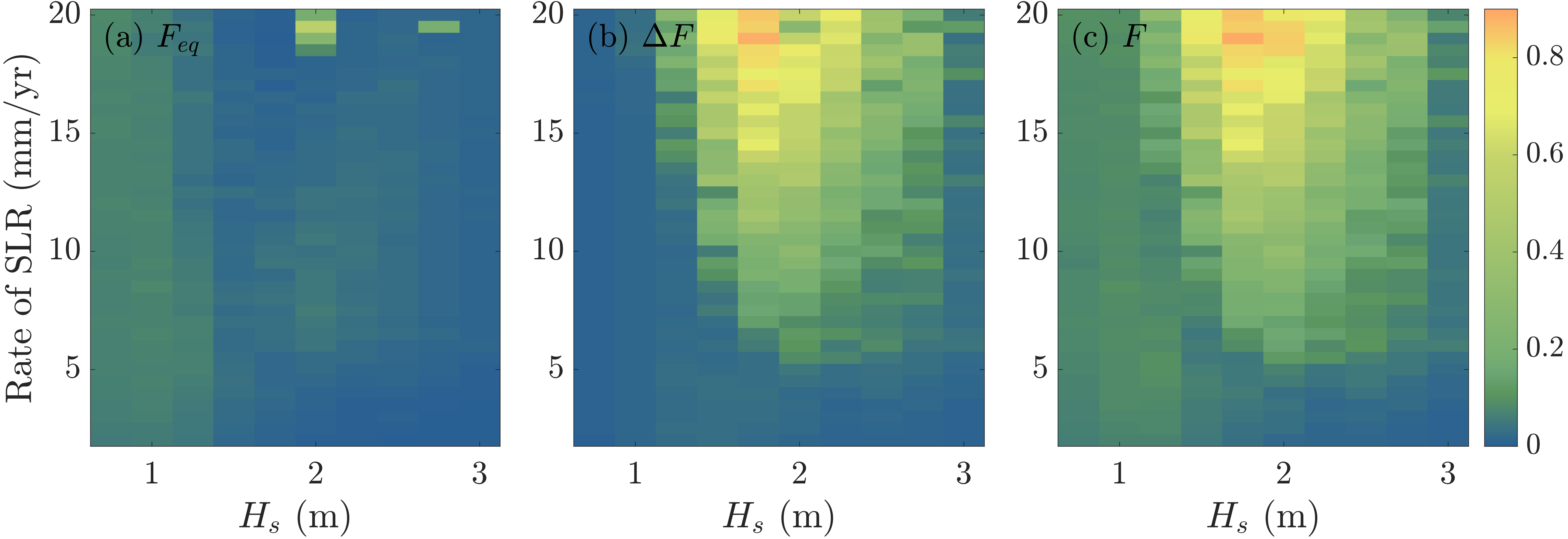

(a) F_{eq}
(b) ΔF
(c) F
Rate of SLR (mm/yr)
20
15
10
5
1
2
3
H_s (m)
0
0.2
0.4
0.6
0.8

Figure 7.

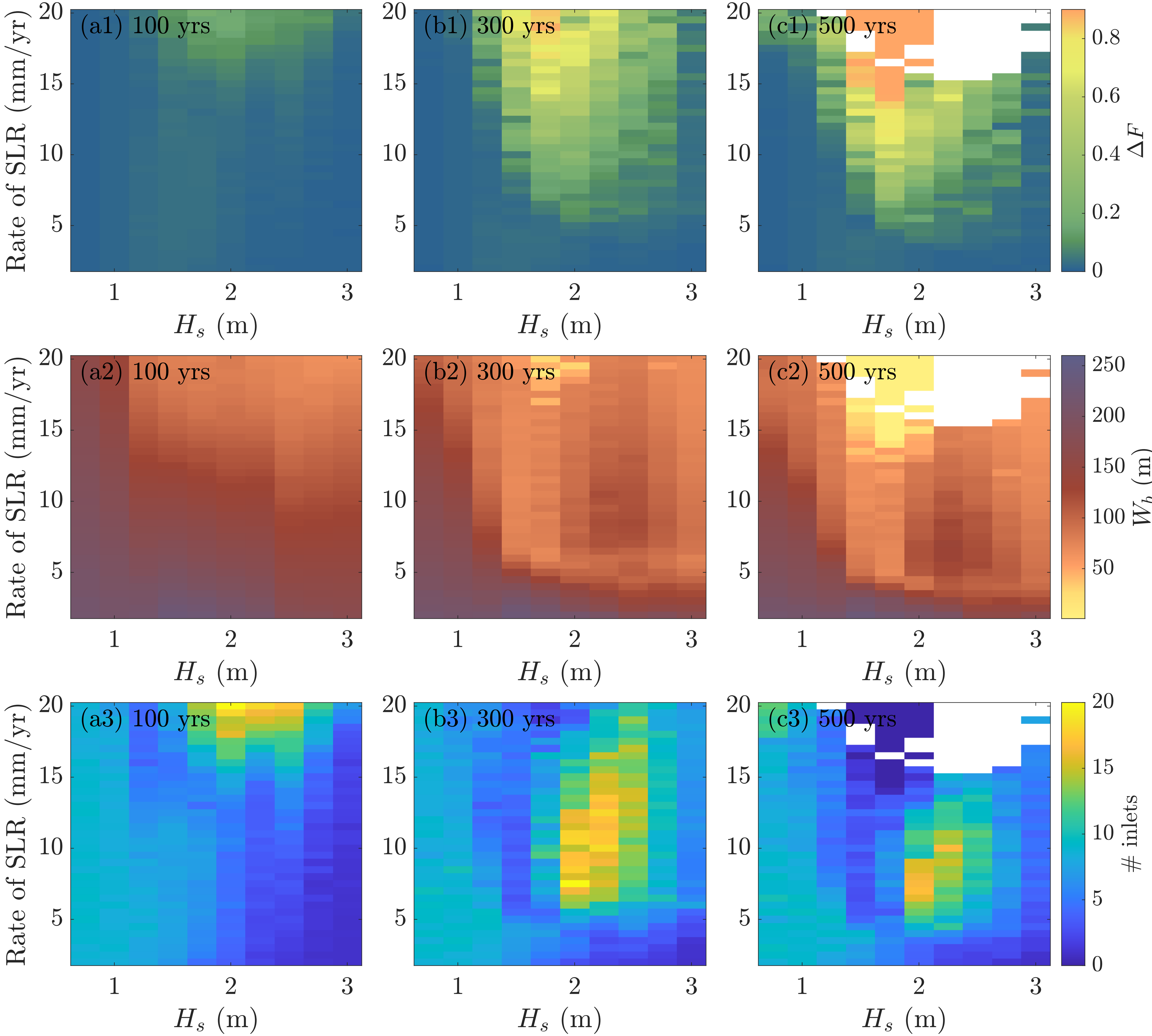

(a1) 100 yrs
(b1) 300 yrs
(c1) 500 yrs
(a2) 100 yrs
(b2) 300 yrs
(c2) 500 yrs
(a3) 100 yrs
(b3) 300 yrs
(c3) 500 yrs
Rate of SLR (mm/yr)
H_s (m)
ΔF
W_b (m)
inlets

Figure 8.

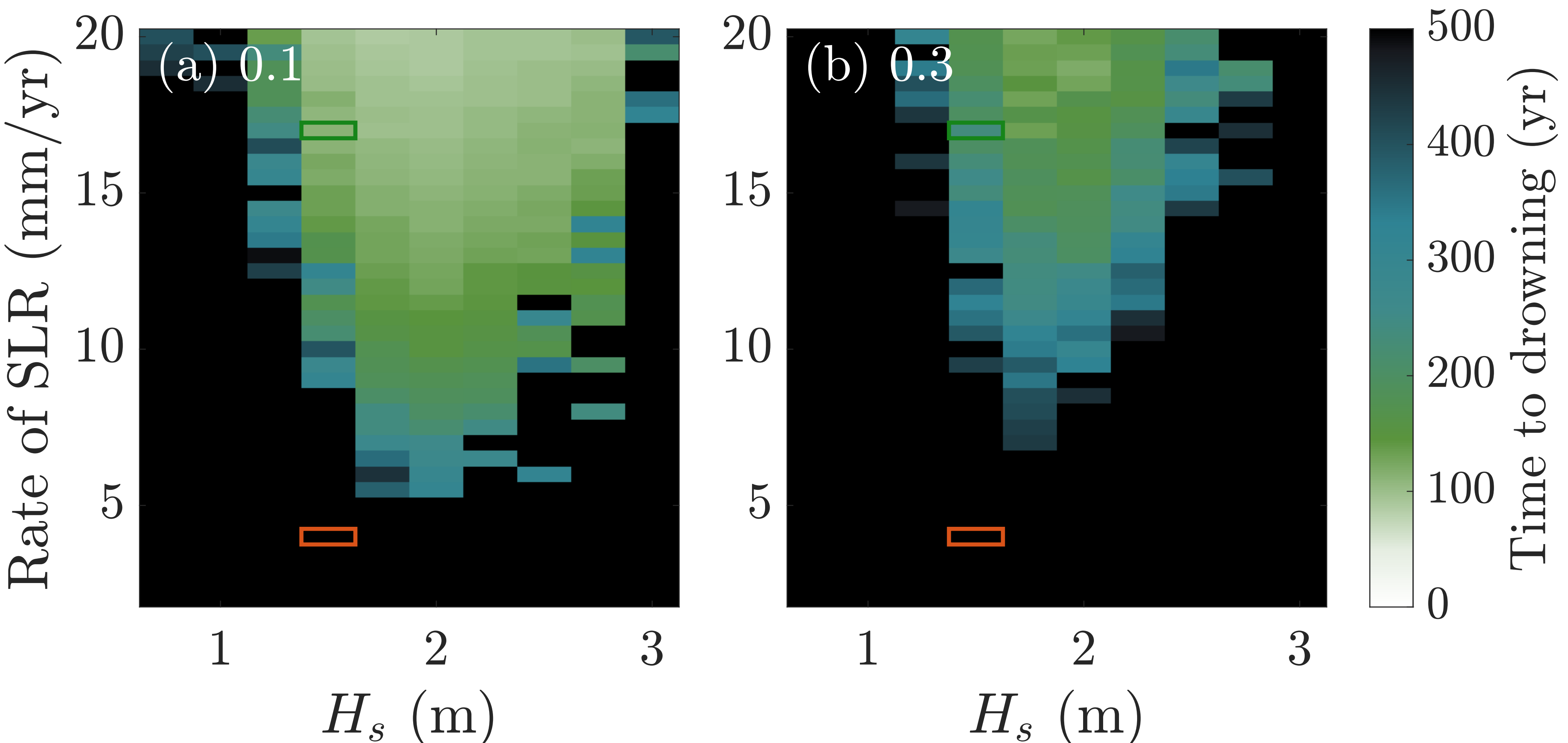

(a) 0.1
(b) 0.3
Rate of SLR (mm/yr)
20
15
10
5
1
2
3
H_s (m)
Time to drowning (yr)
500
400
300
200
100
0

Figure 9.

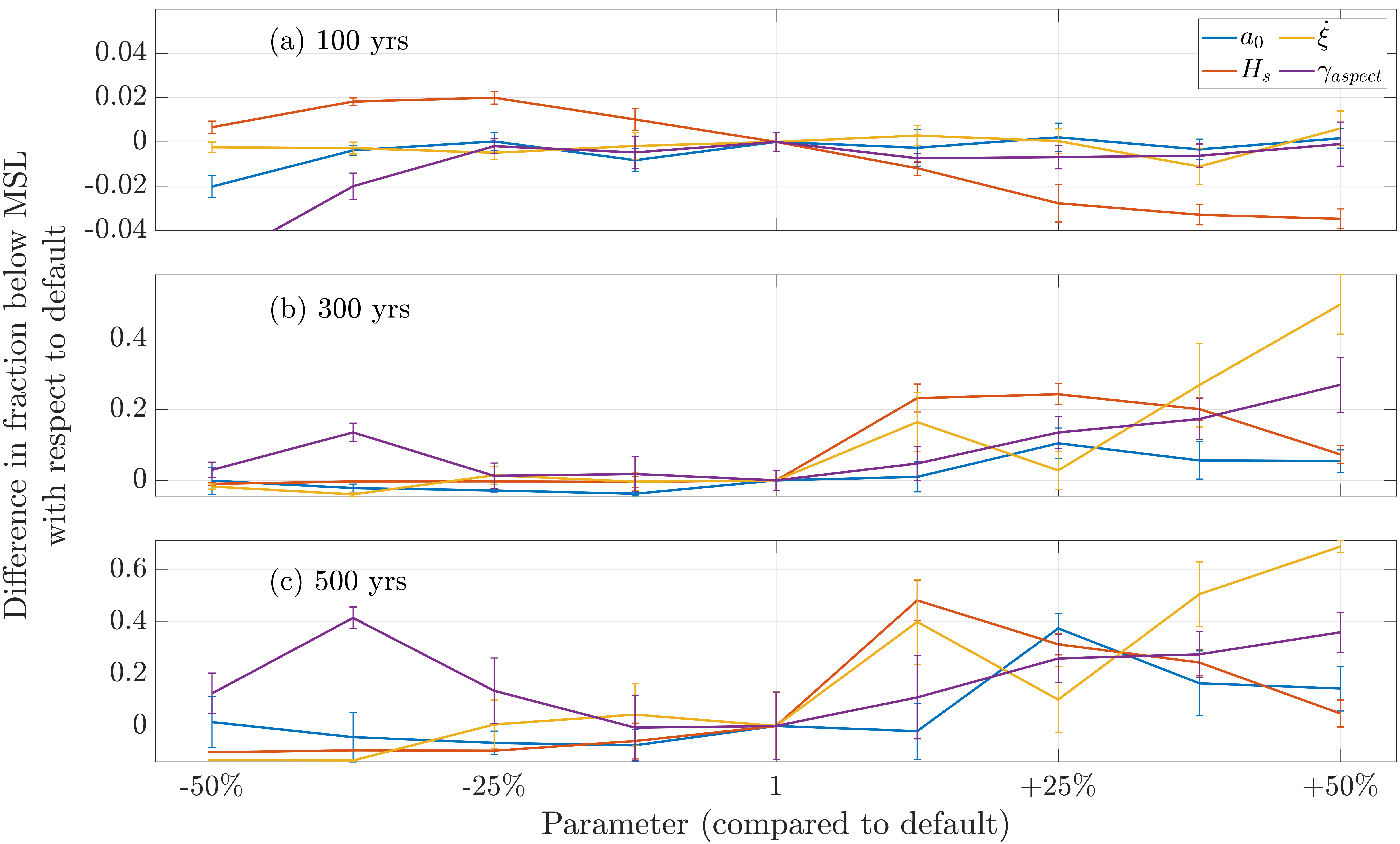

(a) 100 yrs
(b) 300 yrs
(c) 500 yrs
a_0
$\dot{\xi}$
H_s
γ_{aspect}
0.04
0.02
0
-0.02
-0.04
0.4
0.2
0
0.6
0.4
0.2
0
-50%
-25%
1
+25%
+50%
Parameter (compared to default)
Difference in fraction below MSL
with respect to default